ELSEVIER

Contents lists available at ScienceDirect

# Journal of Theoretical Biology

journal homepage: www.elsevier.com/locate/yjtbi





# A multi-strain model with asymptomatic transmission: Application to COVID-19 in the US

Shasha Gao a,b, Mingwang Shen c, Xueying Wang d, Jin Wang e, Maia Martcheva b, Libin Rong b,\*

- a School of Mathematics and Statistics, Jiangxi Normal University, Nanchang, 330000, China
- <sup>b</sup> Department of Mathematics, University of Florida, Gainesville, FL 32611, United States of America
- c China-Australia Joint Research Centre for Infectious Diseases, School of Public Health, Xi'an Jiaotong University Health Science Center, Xi'an, Shaanxi, China
- d Department of Mathematics and Statistics, Washington State University, Pullman, WA 99163, United States of America
- <sup>e</sup> Department of Mathematics, University of Tennessee at Chattanooga, Chattanooga, TN 37403, United States of America

# ARTICLE INFO

#### Keywords: COVID-19 Multi-strain model Asymptomatic transmission Control measures

#### ABSTRACT

COVID-19, induced by the SARS-CoV-2 infection, has caused an unprecedented pandemic in the world. New variants of the virus have emerged and dominated the virus population. In this paper, we develop a multistrain model with asymptomatic transmission to study how the asymptomatic or pre-symptomatic infection influences the transmission between different strains and control strategies that aim to mitigate the pandemic. Both analytical and numerical results reveal that the competitive exclusion principle still holds for the model with the asymptomatic transmission. By fitting the model to the COVID-19 case and viral variant data in the US, we show that the omicron variants are more transmissible but less fatal than the previously circulating variants. The basic reproduction number for the omicron variants is estimated to be 11.15, larger than that for the previous variants. Using mask mandate as an example of non-pharmaceutical interventions, we show that implementing it before the prevalence peak can significantly lower and postpone the peak. The time of lifting the mask mandate can affect the emergence and frequency of subsequent waves. Lifting before the peak will result in an earlier and much higher subsequent wave. Caution should also be taken to lift the restriction when a large portion of the population remains susceptible. The methods and results obtained her e may be applied to the study of the dynamics of other infectious diseases with asymptomatic transmission using other control measures.

# 1. Introduction

Coronavirus disease-2019 (COVID-19) is a novel infectious disease caused by the SARS-CoV-2 virus, which can be spread from person to person (World Health Organization, 2022). This virus is highly contagious and has swept the globe. Even though a lot of infected people are asymptomatic, or only experience mild to moderate symptoms, some develop a serious illness or even die, especially among older people or those with underlying medical conditions. According to the World Health Organization (WHO), more than 521 million confirmed cases of COVID-19, including over 6 million deaths, have been reported by May 2022 (World Health Organization, 2022).

Since COVID-19 was first reported in December 2019 in Wuhan, many effective control strategies have been adopted aiming to prevent or slow down the transmission, such as mask mandate, social distancing, vaccination, travel restriction, lockdown, etc (Howard et al., 2021; Mathieu et al., 2021; Tang, 2022). However, the pandemic is still going on in many countries and has caused devastating damage to public

health and the social economy. One of the reasons why COVID-19 is hard to tackle is that many infected people are asymptomatic but they can infect others without knowing it. Another reason is that the virus continuously mutates. Multiple variants of SARS-CoV-2 have emerged and have been circulating around the world since the beginning of the COVID-19 pandemic, such as alpha, delta, omicron, etc (World Health Organization, 2022). This has brought more challenges as the vaccines or treatments are less effective for the new variants. As more variants appear, which strain might dominate the virus population? Does asymptomatic transmission affect the competition between strains? When should we impose or lift non-pharmaceutical interventions? Does the time of starting or lifting the restrictions affect the spread of COVID-19? The answers to these questions are still vague and need to be further investigated.

Multi-strain mathematical models have been widely used to investigate the infectious disease dynamics (Massard et al., 2022; de León et al., 2022; Li et al., 2021b; Rong et al., 2007, 2012; Li et al., 2021a,

E-mail address: libinrong@ufl.edu (L. Rong).

<sup>\*</sup> Corresponding author.

2013; Martcheva, 2009; Li et al., 2010; Saucedo and Martcheva, 2017; Dang et al., 2016; Duan et al., 2018; Cai et al., 2013; Martcheva and Li, 2013; Martcheva, 2007; Thomasey and Martcheva, 2008; Iannelli et al., 2005; Martcheva et al., 2007; Martcheva and Pilyugin, 2006; Oiu et al., 2013; Martcheva et al., 2008; Arruda et al., 2021; Fudolig and Howard, 2020; Murall et al., 2014; Poolman et al., 2008). Most studied the existence and stability of the disease-free equilibrium (DFE), strain-dominant equilibria and coexistence equilibria. The competitive exclusion principle was also discussed in different circumstances from between-host level to within-host level (Martcheva and Li, 2013; Saucedo and Martcheva, 2017; Dang et al., 2016; Duan et al., 2018; Cai et al., 2013; Rong et al., 2007, 2012). For example, from the between-host level, Martcheva and Li showed that the competitive exclusion principle holds in an infection-age structured model with environmental transmission (Martcheva and Li, 2013). At the withinhost level, a multi-strain model was developed to explain the rapid emergence of drug resistance in HCV patients and discussed which strain(s) would dominate the virus population (Rong et al., 2012). Vaccine-induced strain replacement is another topic investigated by multi-strain models (Martcheva et al., 2008; Iannelli et al., 2005; Thomasey and Martcheva, 2008; Murall et al., 2014; Poolman et al., 2008). In Martcheva et al. (2008), Martcheva et al. reviewed this topic and drew an analogy with ecological and evolutionary explanations for competitive dominance and coexistence. They showed that both perfect and imperfect vaccination may lead to type replacement.

Before the emergence of COVID-19, some papers have studied asymptomatic infection using mathematical models (Saad-Roy et al., 2020; Cai et al., 2017; Hsu and Hsieh, 2008; Robinson and Stilianakis, 2013; Al-Darabsah and Yuan, 2018; Chisholm et al., 2018). For example, Saad-Roy et al. compared fully asymptomatic, less symptomatic, and fully symptomatic first stages, and found bistability between zero and maximal asymptomatic behavior (Saad-Roy et al., 2020). Bistability was also found in Hsu and Hsieh (2008). Cai et al. discussed optimal control of a malaria model with asymptomatic class and superinfection (Cai et al., 2017). They showed that control strategies would always decrease symptomatic infection but might increase asymptomatic infection. Since COVID-19 started, a lot of studies have addressed the asymptomatic infection (Massard et al., 2022; de León et al., 2022; Li et al., 2021b; Knock et al., 2021; Sonabend et al., 2021; Subramanian et al., 2021; Park et al., 2020; Musa et al., 2022; Ngonghala et al., 2020; Shen et al., 2021a,b; He et al., 2021; Calleri et al., 2021; Huo et al., 2021; Rocha Filho et al., 2021; Anggriani et al., 2022; Srivastav et al., 2021; Ahmed et al., 2021; Bugalia et al., 2020; Serhani and Labbardi, 2021; Ali et al., 2020), among which some discussed the role of asymptomatic infection in the transmission of COVID-19 (Subramanian et al., 2021; Park et al., 2020; Huo et al., 2021; Ali et al., 2020). For example, Subramanian et al. found that many infections are asymptomatic but they contribute substantially to the community transmission of COVID-19 (Subramanian et al., 2021). Similar results were shown in Huo et al. (2021). In addition, many studies discussed control strategies including vaccination, lockdown, mask mandate etc (Knock et al., 2021; Sonabend et al., 2021; Ngonghala et al., 2020; He et al., 2021; Shen et al., 2021a,b; Calleri et al., 2021; Srivastav et al., 2021; Bugalia et al., 2020; Serhani and Labbardi, 2021). Knock et al. found that to lift nonpharmaceutical interventions without causing a resurgence of transmission, a high degree of protection and high coverage would be needed for any vaccination campaign (Knock et al., 2021). Ngonghala et al. showed that wearing face masks in public would be very useful in minimizing community transmission of COVID-19 (Ngonghala et al., 2020). In a previous paper (He et al., 2021), we found that timely screening and detection in the early stage of the infection could prevent the occurrence of a future wave. Besides, reducing the size of the susceptible population is critical in mitigating the outbreak of COVID-19.

There is little literature that investigates multi-strain models assuming asymptomatic individuals are infectious. A recently published paper

formulated a multi-strain COVID-19 model and applied it to French data (Massard et al., 2022). They found that beta and gamma variants were more transmissible than the original virus and might result in a large number of infections in France. Another paper studied a twostrain model with vaccination (de León et al., 2022). They predicted the rise of the alpha variant and obtained the minimum vaccine coverage to decelerate the rise of a multi-strain pandemic. Using data from the US, Li et al. also formulated a two-strain model considering infectious asymptomatic class, vaccination, social distancing, face mask etc (Li et al., 2021b). They found that if COVID-19 vaccines remain effective against the SARS-CoV-2 variants, then 70% vaccination coverage would be sufficient to restore social activities to a pre-pandemic level. All these papers computed the reproduction number and did sensitivity analysis. However, they did not conduct any other mathematical analysis for the models. In this paper, using the data from the US, we will study a multi-strain model with infectious asymptomatic classes to investigate the dynamic of COVID-19 transmission both analytically and numerically. Specifically, we will mainly address the following questions: (1) Will infectious asymptomatic class influence the competition between different strains? (2) Will the way of implementing control strategies affect the transmission of COVID-19? The model will be formulated and analyzed in Sections 2 and 3, respectively. By fitting the COVID-19 case and variant data from the US using our model, we conduct a variety of simulations to investigate the competitive exclusion principle and the impact of control strategies in Section 4. Conclusions and discussions are followed in Section 5.

#### 2. Model formulation

In this section, we formulate a multi-strain model to investigate the competition between viral strains during the transmission of COVID-19. The population is divided into 2n + 2 classes: susceptible individuals (S), asymptomatic/pre-symptomatic individuals infected with strain i ( $A_i$ , i = 1, 2, ..., n), symptomatic individuals infected with strain i $(I_i, i = 1, 2, ..., n)$ , and recovered individuals (R). Asymptomatic/presymptomatic infected individuals can also transmit the disease (He et al., 2020; Subramanian et al., 2021). We assume that newborns are susceptible to all COVID-19 strains and enter the susceptible compartment S with the recruitment rate  $\Lambda$ . Susceptible individuals get infected by strain i with the force of infection  $\lambda_i$  and move to the asymptomatic/pre-symptomatic infectious compartment  $A_i$ . Then they may develop symptoms and move to the symptomatic infected class  $I_i$  at a rate  $\alpha_i$ . Both asymptomatic/pre-symptomatic infected individuals in class  $A_i$  and symptomatic infected individuals in class  $I_i$  can recover at rates  $\gamma_{A_i}$  and  $\gamma_{I_i}$ , respectively. All of them can leave their compartments by a natural death at a rate  $\mu$ . In addition, symptomatic infected individuals in class  $I_i$  can die due to the disease at a rate  $\omega_i$ . A flow chart of the model is shown in Fig. 1. The detailed descriptions of variables and parameters are given in Table 1.

It is worth noting that we adopt the SAIR (susceptible-asymptomatic infected-symptomatic infected-recovered) modeling framework in this paper. The asymptomatic and pre-symptomatic individuals are grouped into one class. Because we are more interested in studying the competition between different strains and the impact of the way of implementing control strategies, we use a simple modeling framework and do not consider the exposed class, which was also ignored in some other COVID-19 papers (Massard et al., 2022; Calleri et al., 2021; Serhani and Labbardi, 2021). In view of the observation that the breakthrough infection or reinfection only accounts for a small portion of the total infection, we assume the acquired immunity to be permanent after recovery, which was also the assumption in many other papers of COVID-19 (Massard et al., 2022; Calleri et al., 2021; Serhani and Labbardi, 2021; Huo et al., 2021; Musa et al., 2022; Shen et al., 2021a,b; Li et al., 2021b). If we add more classes such as the exposed class, the basic reproduction numbers and the dynamics of the model will be slightly different from that obtained using the current

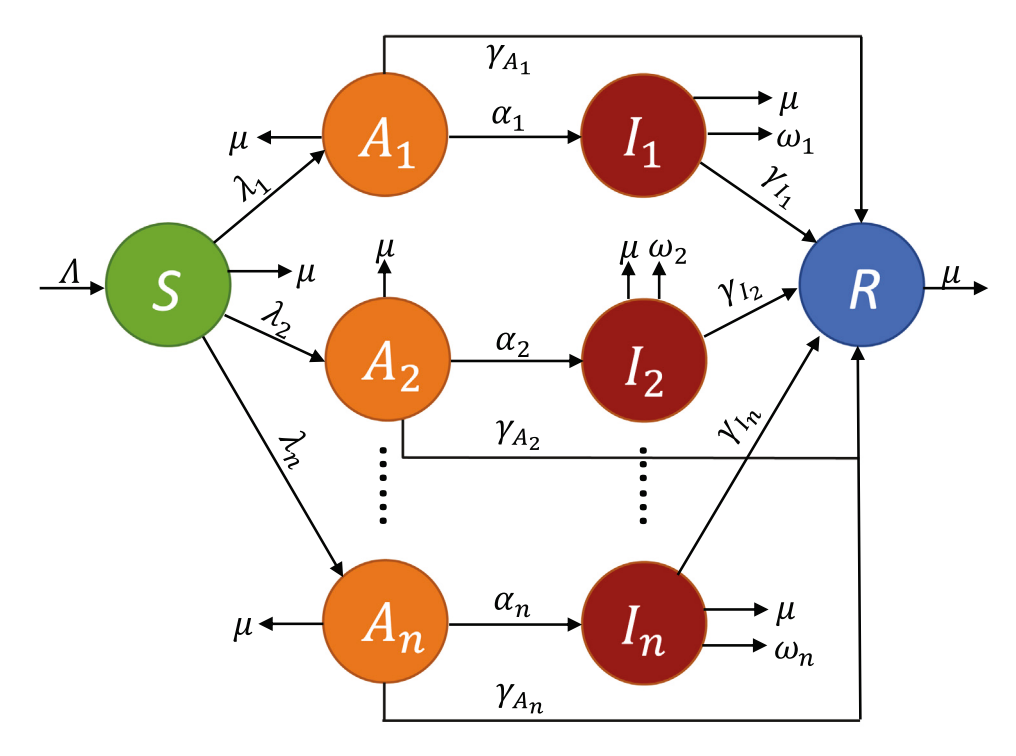


Fig. 1. Flow diagram of the model of COVID-19 transmission. The population is divided into 2n+2 classes: susceptible individuals (S), asymptomatic/pre-symptomatic individuals infected with strain i ( $A_i$ ,  $i=1,2,\ldots,n$ ), symptomatic individuals infected with strain i ( $I_i$ ,  $i=1,2,\ldots,n$ ), and recovered individuals (R). Asymptomatic/pre-symptomatic infected individuals can also transmit the disease. Descriptions of parameters are given in Table 1.

model. For example, the prevalence peak will be slightly delayed when including the exposed class. If we use the SAIRS modeling framework by considering waning immunity after recovery, the basic reproduction number will remain the same, but the prevalence peak will be earlier and higher.

$$\begin{cases} S'(t) = A - S \sum_{i=1}^{n} \lambda_{i} - \mu S, \\ A'_{i}(t) = \lambda_{i} S - (\alpha_{i} + \gamma_{A_{i}} + \mu) A_{i}, & i = 1, 2, \dots, n, \\ I'_{i}(t) = \alpha_{i} A_{i} - (\omega_{i} + \gamma_{I_{i}} + \mu) I_{i}, & i = 1, 2, \dots, n, \\ R'(t) = \sum_{i=1}^{n} (\gamma_{A_{i}} A_{i} + \gamma_{I_{i}} I_{i}) - \mu R. \end{cases}$$

$$(1)$$

The force of infection is given by

$$\lambda_i = \beta_{A_i} A_i + \beta_{I_i} I_i.$$

For convenience, we denote

$$\delta_{A_i} = \alpha_i + \gamma_{A_i} + \mu, \qquad \delta_{I_i} = \omega_i + \gamma_{I_i} + \mu.$$

Taking the sum of equations in system (1), we get  $N' \leq \Lambda - \mu N$ , where  $N = S + \sum_{i=1}^{n} (A_i + I_i) + R$  is the total population. We define the domain of the system (1) to be

$$\varOmega = \left\{ (S, A_1, A_2, \dots, A_n, I_1, I_2, \dots, I_n, R) \in \Re^{2n+2} \, : \, S + \sum_{i=1}^n (A_i + I_i) + R \leq \Lambda/\mu \right\}.$$

Using a similar method as in our previous study (Gao et al., 2021), we can verify that  $\Omega$  is positively invariant for system (1) and the model is both epidemiologically and mathematically well-posed.

# 3. Analysis

# 3.1. Two-strain model

We first consider the two-strain case (n = 2). The system (1) can be reduced to the following system:

$$\begin{cases} S'(t) = A - S(\lambda_1 + \lambda_2) - \mu S, \\ A'_1(t) = \lambda_1 S - \delta_{A_1} A_1, \\ I'_1(t) = \alpha_1 A_1 - \delta_{I_1} I_1, \\ A'_2(t) = \lambda_2 S - \delta_{A_2} A_2, \\ I'_2(t) = \alpha_2 A_2 - \delta_{I_2} I_2, \\ R'(t) = \sum_{i=1}^{2} (\gamma_{A_i} A_i + \gamma_{I_i} I_i) - \mu R, \end{cases}$$
(2)

where  $\lambda_i$ ,  $\delta_{A_i}$  and  $\delta_{I_i}$  with i = 1, 2 are defined the same as before.

# 3.1.1. Basic reproduction numbers and disease-free equilibrium

The system (2) always has a unique disease-free equilibrium (DFE)  $E_0^*=(S_0^*,0,0,0,0,0)$ , where  $S_0^*=\frac{\Lambda}{\mu}$ . Using the next-generation matrix approach Appendix A, we define the basic reproduction number to be

$$\mathcal{R}_0 = \max\{\mathcal{R}_{0,1}, \mathcal{R}_{0,2}\}$$

where  $\mathcal{R}_{0,i} = \mathcal{R}_{0,i}^A + \mathcal{R}_{0,i}^I$  with

$$\mathcal{R}^A_{0,i} = \frac{S^*_0\beta_{A_i}}{\delta_{A_i}}, \quad \mathcal{R}^I_{0,i} = \frac{S^*_0\beta_{I_i}\alpha_i}{\delta_{A_i}\delta_{I_i}}, \quad i=1,2.$$

Considering the biological interpretation of  $\mathcal{R}_{0,1}$ , we set  $A_1$  to be 1 in the incidence term  $\beta_{A_1}SA_1$ . Then  $\beta_{A_1}S_0^*$  represents the number of secondary infections generated by one infectious individual who is in class  $A_1$  in an entirely susceptible population per unit of time.  $1/\delta_{A_1}$  is the average time spent by an infectious individual in class  $A_1$ . Thus,  $\mathcal{R}_{0,1}^A$  represents the number of secondary infections generated by one infectious individual when he/she is in class  $A_1$  in an entirely susceptible

Descriptions of variables and parameters.

Symbol	Description	Baseline	Unit	Range	Source	
Variables						
S(t)	Susceptible population					
$A_i(t)$	Asymptomatic/pre-symptomatic population of strain i					
$I_i(t)$	Symptomatic population of strain i					
R(t)	Recovered population					
N(t)	Total population					
$\lambda_i(t)$	Force of infection of strain i					
Parameters						
Λ	Recruitment rate	11528	person/day	Fixed	See tex	
μ	Natural death rate	1/(79*365)	1/day	Fixed	See tex	
$\beta_{A_i}$	Asymptomatic transmission rate of strain i	Fitted	1/(person*day)	Fitted		
$\beta_{I_i}$	Symptomatic transmission rate of strain i	Fitted	1/(person*day)	Fitted		
$\alpha_{i}^{'}$	Transition rate from $A_i$ to $I_i$	Fitted	1/day	Fitted		
$\gamma_{A_i}$	Recovery rate of $A_i$	Fitted	1/day	Fitted		
$\gamma_{I_i}$	Recovery rate of $I_i$	Fitted	1/day	Fitted		
$\omega_i$	Disease-induced death rate of $I_i$	Fitted	1/day	Fitted		
e	Mask efficacy	Varied	unitless	[0, 1]		
c	Mask coverage	Varied	unitless	[0, 1]		

population.  $\alpha_1/\delta_{A_1}$  represents the fraction of infectious individuals who survive from the asymptomatic/pre-symptomatic stage and move to the class  $I_1$ . Therefore,  $\mathcal{R}_{0,1}^I$  represents the number of secondary infections generated by one infectious individual when he/she is in class  $I_1$  in an entirely susceptible population. It follows that  $\mathcal{R}_{0,1}$  represents the number of secondary infections generated by one infectious individual of strain 1 during his/her whole infectious period in an entirely susceptible population.  $\mathcal{R}_{0,2}$  has the similar interpretation.

Since  $\mathcal{R}_0$  is derived using the next generation matrix approach, according to Van den Driessche and Watmough (2002), we have the following local stability for the DFE:

**Theorem 1.** When  $\mathcal{R}_0 < 1$  (i.e.  $\mathcal{R}_{0,1} < 1$  and  $\mathcal{R}_{0,2} < 1$ ), the DFE  $E_0^*$  is locally asymptotically stable; when  $\mathcal{R}_0 > 1$  (i.e.  $\mathcal{R}_{0,1} > 1$  or  $\mathcal{R}_{0,2} > 1$ ), the DFE  $E_0^*$  is unstable.

We further have the global stability for the DFE as follows. The proof is given in Appendix B.

**Theorem 2.** When  $\mathcal{R}_0 \leq 1$  (i.e.  $\mathcal{R}_{0,1} \leq 1$  and  $\mathcal{R}_{0,2} \leq 1$ ), the DFE  $E_0^*$  is globally asymptotically stable.

Recall that the basic reproduction number represents the number of secondary infections generated by one infectious individual in a wholly susceptible environment. The above two theorems indicate that if the basic reproduction numbers for both strains are reduced to less than or equal to 1, the disease will eventually die out no matter how many susceptible, asymptomatic, symptomatic, and recovered individuals there are now. However, if the basic reproduction number of any strain is greater than 1, the disease may not be eradicated.

## 3.1.2. Strain-dominant equilibrium

In this section, we consider the strain-dominant equilibria. The results on their existence are shown in the following theorem with the proof given in Appendix C.

**Theorem 3.** When  $\mathcal{R}_{0,1} > 1$ , there exists a unique strain-1-dominant equilibrium  $E_1^* = (S_1^*, A_1^*, I_1^*, 0, 0, R_1^*)$ ; When  $\mathcal{R}_{0,2} > 1$ , there exists a unique strain-2-dominant equilibrium  $E_2^* = (S_2^*, 0, 0, A_2^*, I_2^*, R_2^*)$ , where

$$\begin{split} S_i^* &= \frac{\varLambda}{\mu} \frac{1}{\mathcal{R}_{0,i}}, \qquad A_i^* &= \frac{\varLambda}{\delta_{A_i}} \bigg( 1 - \frac{1}{\mathcal{R}_{0,i}} \bigg), \\ I_i^* &= \frac{\alpha_i}{\delta_{I_i}} A_i^*, \qquad R_i^* &= \frac{1}{\mu} \bigg( \gamma_{A_i} + \gamma_{I_i} \frac{\alpha_i}{\delta_{I_i}} \bigg) A_i^*, \end{split}$$

with i = 1, 2.

Concerning the stability of the strain-dominant equilibria, we have the following results with proofs given in Appendix D and Appendix E, respectively.

**Theorem 4.** (i) Suppose that  $\mathcal{R}_{0,1} > 1$ . When  $\mathcal{R}_{0,1} > \mathcal{R}_{0,2}$ , the strain-1-dominant equilibrium  $E_1^*$  is locally asymptotically stable; when  $\mathcal{R}_{0,1} < \mathcal{R}_{0,2}$ ,  $E_1^*$  is unstable.

(ii) Suppose that  $\mathcal{R}_{0,2} > 1$ . When  $\mathcal{R}_{0,2} > \mathcal{R}_{0,1}$ , the strain-2-dominant equilibrium  $E_2^*$  is locally asymptotically stable; when  $\mathcal{R}_{0,2} < \mathcal{R}_{0,1}$ ,  $E_2^*$  is unstable.

**Theorem 5.** (i) Suppose that  $\mathcal{R}_{0,1} > 1$ . When  $\mathcal{R}_{0,1} > \mathcal{R}_{0,2}$ , the strain-1-dominant equilibrium  $E_1^*$  is globally asymptotically stable.

(ii) Suppose that  $\mathcal{R}_{0,2} > 1$ . When  $\mathcal{R}_{0,2} > \mathcal{R}_{0,1}$ , the strain-2-dominant equilibrium  $E_2^*$  is globally asymptotically stable.

Theorems 3, 4, and 5 show that when an infected individual with strain i leads to more than one new infection, we have the strain-i-dominant steady state  $E_i^*$ , in which there is only the infection with strain i (i = 1 or 2). Furthermore, if an infected individual with strain i leads to more infections than the other strain, this steady state  $E_i^*$  will be the final state of the disease, no matter what the current infection status is.

#### 3.1.3. Interior or coexistence equilibrium

From the previous section, we can see that coexistence of the two strains is not possible when  $\mathcal{R}_{0,1}\neq\mathcal{R}_{0,2}$ . In the special case  $\mathcal{R}_{0,1}=\mathcal{R}_{0,2}$ , we have the following result. The proof is given in Appendix F.

**Theorem 6.** When  $\mathcal{R}_{0,1} = \mathcal{R}_{0,2} > 1$ , there exist infinitely many interior equilibria  $E^*$ .

This theorem shows that if the two strains have the same infection ability and an infectious individual can induce more than one new infection, there will be infinitely many steady states involving the infection of both strains. Which steady state will be ended up with depends on where the infection starts.

#### 3.2. General case: n strains

In this section, we consider the general case (i.e. the model with n strains). System (1) always has a unique disease-free equilibrium

$$E_0^{**} = \left(\frac{\Lambda}{\mu}, \underbrace{0, \dots, 0}_{2n+1}\right).$$

Similar to the two-strain case, by the next-generation matrix approach we define the basic reproduction number for strain i to be

$$\mathcal{R}_{0,i} = \frac{\Lambda \beta_{A_i}}{\mu \delta_{A_i}} + \frac{\Lambda \alpha_i \beta_{I_i}}{\mu \delta_{A_i} \delta_{I_i}}, \quad i = 1, 2, \dots, n.$$

Then

$$\mathcal{R}_0 = \max \{\mathcal{R}_{0,1}, \dots, \mathcal{R}_{0,n}\}.$$

For the existence and stability of equilibria, we have the following results. Since the proofs are similar to the two-strain case, we omit them.

**Theorem 7.** When  $\mathcal{R}_0 \leq 1$  (i.e.  $\mathcal{R}_{0,i} \leq 1$  for all  $i=1,2,\ldots,n$ ), the DFE  $E_0^{**}$  is globally asymptotically stable; when  $\mathcal{R}_0 > 1$  (i.e.  $\mathcal{R}_{0,i} > 1$  for some  $i=1,2,\ldots,n$ ), the DFE  $E_0^{**}$  is unstable.

**Theorem 8.** When  $\mathcal{R}_{0,i} > 1$   $(i = 1, 2, \dots, n)$ , there is a unique strain-idominant equilibrium  $E_i^{**} = (S_i^{**}, 0, \dots, 0, A_i^{**}, I_i^{**}, 0, \dots, 0, R_i^{**})$ , where

$$\begin{split} S_i^{**} &= \frac{\Lambda}{\mu} \frac{1}{\mathcal{R}_{0,i}}, \qquad A_i^{**} &= \frac{\Lambda}{\delta_{A_i}} \bigg( 1 - \frac{1}{\mathcal{R}_{0,i}} \bigg), \\ I_i^{**} &= \frac{\alpha_i}{\delta_{I_i}} A_i^{**}, \qquad R_i^{**} &= \frac{1}{\mu} \bigg( \gamma_{A_i} + \gamma_{I_i} \frac{\alpha_i}{\delta_{I_i}} \bigg) A_i^{**}. \end{split}$$

**Theorem 9.** Suppose that  $\mathcal{R}_{0,i} > 1$  for some i. When  $\mathcal{R}_{0,i} > \mathcal{R}_{0,j}$  for all  $j \neq i$  (i.e.  $j = 1, 2, \ldots, i - 1, i + 1, \ldots, n$ ), the strain-i-dominant equilibrium  $E_i^{**}$  is locally and globally asymptotically stable; when  $\mathcal{R}_{0,i} < \mathcal{R}_{0,j}$  for some  $j \neq i$ , the strain-i-dominant equilibrium  $E_i^{**}$  is unstable.

**Theorem 10.** When  $\mathcal{R}_{0,i}$  are equal to each other for all i = 1, 2, ..., n, there exist infinitely many interior equilibria  $E^{**}$ .

# 4. Data fitting and numerical investigation

# 4.1. Data

We collected COVID-19 daily cases and variant proportions for the US from the Centers for Disease Control and Prevention (CDC) (Centers for Disease Control and Prevention (CDC), 2022a). The variant proportions were reported weekly. The first data of omicron proportion was for the week 11/21/2021–11/27/2021. We assigned this data to the middle of the week, i.e. 11/24/2021. Similarly, we obtained the data of omicron proportions for each Wednesday from 11/24/2021 to 1/12/2022. We also collected the daily cases for the same period. Since some states only reported daily cases during weekdays, we used the 7-day average data. The data set is shown in Table 2. The reason we chose this time range is that we are more interested in the transition between strains. Before or after this period, one strain dominates the virus population. Both COVID-19 daily cases and omicron proportions are used for model calibration.

# 4.2. Parameter setting and model calibration

Since the life expectancy for the US population before the pandemic is about 79 years (Centers for Disease Control and Prevention (CDC), 2022b), we fix the natural death rate  $\mu=1/(79*365)~{\rm day}^{-1}$ . The total population in the US in 2021 is  $N_0=332398949$ , which is relatively stable. Therefore, we assume that the birth rate is similar to the natural death rate and roughly estimate the recruitment rate  $\Lambda=N_0*\mu$  with unit person/day. The other parameter values and the initial conditions of System (2) are calibrated using the data from Table 2.

We use the nonlinear least-squares approach to minimize the Root Mean Square Error (RMSE) between data and simulated results for model calibration. Reported data of COVID-19 daily cases and omicron proportions in the US are used in this paper. These two types of data have different orders of magnitude. Therefore, we normalize the data sets by dividing them by the maximum value from each data set. In addition, we have 50 data points for daily cases but only 8 for omicron proportions. Thus, we minimize the sum of the mean square errors for the two data sets instead of the sum of two square errors. In this way, the two data sets have the same weights in the data fitting procedure.

$$RMSE = \sqrt{\sum_{i=1}^{N_1} \frac{(x(t_i) - X_i)^2}{N_1} + \sum_{j=1}^{N_2} \frac{(y(t_j) - Y_j)^2}{N_2}},$$

where the first and the second terms under the square root correspond to daily cases and omicron proportions, respectively.  $X_i$ ,  $Y_j$  represent normalized data values, and  $N_1$ ,  $N_2$  are the numbers of data points in these two data sets, respectively.  $x(t_i)$  and  $y(t_j)$  are normalized simulated values at the same time points corresponding to the data. We use strain 1 and strain 2 to denote the omicron variants and other variants (mainly delta variants), respectively, as observed in the CDC data. It follows that

$$x(t_i) = \frac{\left(\beta_{A_1}A_1(t_i) + \beta_{I_1}I_1(t_i) + \beta_{A_2}A_2(t_i) + \beta_{I_2}I_2(t_i)\right)S(t_i)}{X_{max}}$$

and

$$y(t_j) = \frac{\left(\beta_{A_1} A_1(t_j) + \beta_{I_1} I_1(t_j)\right) S(t_j)}{\left(\beta_{A_1} A_1(t_j) + \beta_{I_1} I_1(t_j) + \beta_{A_2} A_2(t_j) + \beta_{I_2} I_2(t_j)\right) S(t_j) Y_{max}},$$

where

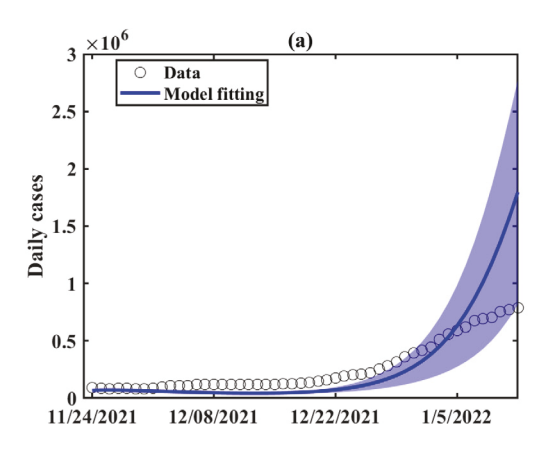
$$X_{max} = \max_{1 \leq i \leq N_1} \{X_i\}, \qquad Y_{max} = \max_{1 \leq j \leq N_2} \{Y_j\}.$$

The fitted parameter values and initial conditions are given in Table 3. We can see that compared with the delta variants, the omicron variants have a higher transmission rate, higher transition rate, similar recovery rates, and lower disease-induced death rate. This indicates that the omicron variants are more transmissible but less fatal than the previously circulating delta variants.

Based on the fitting results from Table 3, we perturbed each parameter and initial condition to generate a band of curves. By conducting several simulations, we notice that those bands corresponding to about 8% perturbation can describe the data variation well with small RMSE. Similar to the procedure used in Li et al. (2021b), we randomly generate 100 small perturbation factors within the range [6%, 10%]. For each perturbation factor a%, we perturb every parameter and initial condition by a% in both positive and negative directions. According to the Latin Hypercube Sampling (LHS) method, we randomly sample 1000 parameter sets within their ranges, which correspond to a band of curves. The number of data points covered by this band and their RMSE can be computed. Then we select the one with the smallest RMSE through the 100 bands. For this selected band, we have 1000 curves, which are used to derive the 95% CI of the model simulation. The results are shown in Fig. 2. Even though the data set for daily cases is within the 95% CI, the fitted line is higher than the real data at the end of this period. There are several possible reasons. For example, as COVID-19 cases arise, more and more people have chosen to get vaccinated or take various non-pharmaceutical interventions, which are not considered explicitly in our model.

# 4.3. Competition between strains

In Section 3, we derived the existence and global stability results for the DFE and strain-dominant equilibria, which are summarized in Fig. 3(a). The circled equilibrium is stable in each region. However, in the special case  $\mathcal{R}_{0,1}=\mathcal{R}_{0,2}$ , we only have the existence for the interior equilibrium  $E^*$ . To numerically investigate the stability of  $E^*$ ,



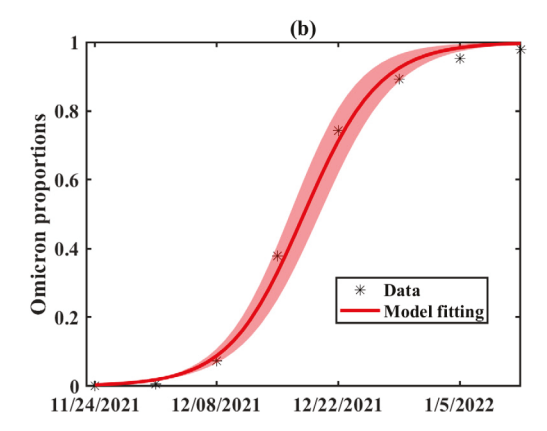


Fig. 2. Model calibration by daily COVID-19 cases and omicron proportions in the US. The results for daily cases and omicron proportions are shown in (a) and (b), respectively. The shaded regions denote the 95% confidence interval. The data set used here is listed in Table 2, which is collected from the US CDC website (Centers for Disease Control and Prevention (CDC), 2022a).

Table 2
Data from the US CDC for model calibration (Centers for Disease Control and Prevention (CDC), 2022a).

Date	Daily cases	Omicron proportion	Date	Daily cases	Omicron proportion
11/24/2021	94590	0.000652581	12/19/2021	138509	
11/25/2021	88653		12/20/2021	150064	
11/26/2021	83917		12/21/2021	162183	
11/27/2021	85313		12/22/2021	176051	0.742894053
11/28/2021	88058		12/23/2021	193066	
11/29/2021	80140		12/24/2021	203403	
11/30/2021	82979		12/25/2021	208404	
12/1/2021	86876	0.006183981	12/26/2021	223643	
12/2/2021	97097		12/27/2021	254622	
12/3/2021	107153		12/28/2021	282107	
12/4/2021	108862		12/29/2021	317018	0.892975569
12/5/2021	108623		12/30/2021	362522	
12/6/2021	121897		12/31/2021	394035	
12/7/2021	122706		1/1/2022	416866	
12/8/2021	122339	0.073683523	1/2/2022	444402	
12/9/2021	121595		1/3/2022	510796	
12/10/2021	119177		1/4/2022	558108	
12/11/2021	118855		1/5/2022	590326	0.952672899
12/12/2021	119270		1/6/2022	618657	
12/13/2021	119510		1/7/2022	674961	
12/14/2021	119283		1/8/2022	694091	
12/15/2021	121520	0.379368961	1/9/2022	702320	
12/16/2021	124647		1/10/2022	756647	
12/17/2021	128529		1/11/2022	768593	
12/18/2021	131965		1/12/2022	789652	0.978338718

Table 3
Fitted parameter values and initial conditions.

Initial condition	Value	Parameter	Value
$S_0$	$9.796 \times 10^{7}$	$\beta_{A_1}$	$1.311 \times 10^{-9}$
$A_{1,0}$	1000	$\beta_{I_1}$	$4.334 \times 10^{-9}$
$I_{1,0}$	300	$\alpha_1$	0.330
$A_{2,0}$	$9.550 \times 10^{5}$	$\omega_1$	0.017
$I_{2,0}$	$8.000 \times 10^{5}$	$\gamma_{A_1}$	0.094
$R_0$	$2.327 \times 10^{8}$	$\gamma_{I_1}$	0.094
		$oldsymbol{eta}_{A_2}$	$1.626 \times 10^{-10}$
		$\beta_{I_2}$	$6.703 \times 10^{-10}$
		$\alpha_2$	0.200
		$\omega_2$	0.021
		$\gamma_{A_2}$	0.091
		$\gamma_{I_2}$	0.091

we choose the fitted parameter values for strain 1 (see Table 3) and set parameter values for strain 2 to be the same as strain 1. In this case,  $\mathcal{R}_{0,1} = \mathcal{R}_{0,2} = 11.1505$ . In Fig. 3(b-d), we assign different initial

conditions. The results show that there are multiple stable interior equilibria when  $\mathcal{R}_{0,1}=\mathcal{R}_{0,2}.$ 

In Fig. 4(a), we use the fitted parameter values (see Table 3) with  $\mathcal{R}_{0,1}$  = 11.1505 and  $\mathcal{R}_{0,2}$  = 1.5547. It shows that the strain-1-dominant equilibrium  $E_1^*$  exists and is stable. These numerical results support the observation that the omicron variants outcompete the previously circulating variants and dominate the virus population eventually as it has a larger basic reproduction number. According to the analytical results of the deterministic model (2), the disease-free equilibrium is unstable and the disease will persist when  $R_{0.1} > 1$  or  $R_{0.2} > 1$ . However, this might not be the case in reality. One of the reasons is that stochasticity can play an important role, especially at the beginning of the outbreak. Using a corresponding stochastic model (Table 4), we show that the system may approach the disease-free equilibrium quickly even when  $\mathcal{R}_{0,1} > 1$  and  $\mathcal{R}_{0,2} > 1$  (Fig. 4(b)). Here we used the same parameter values and initial conditions as in the deterministic model (Fig. 4(a)). This indicates that although the disease spreads fast, it may still have a chance to die out if intervention measures are administered quickly in the beginning.

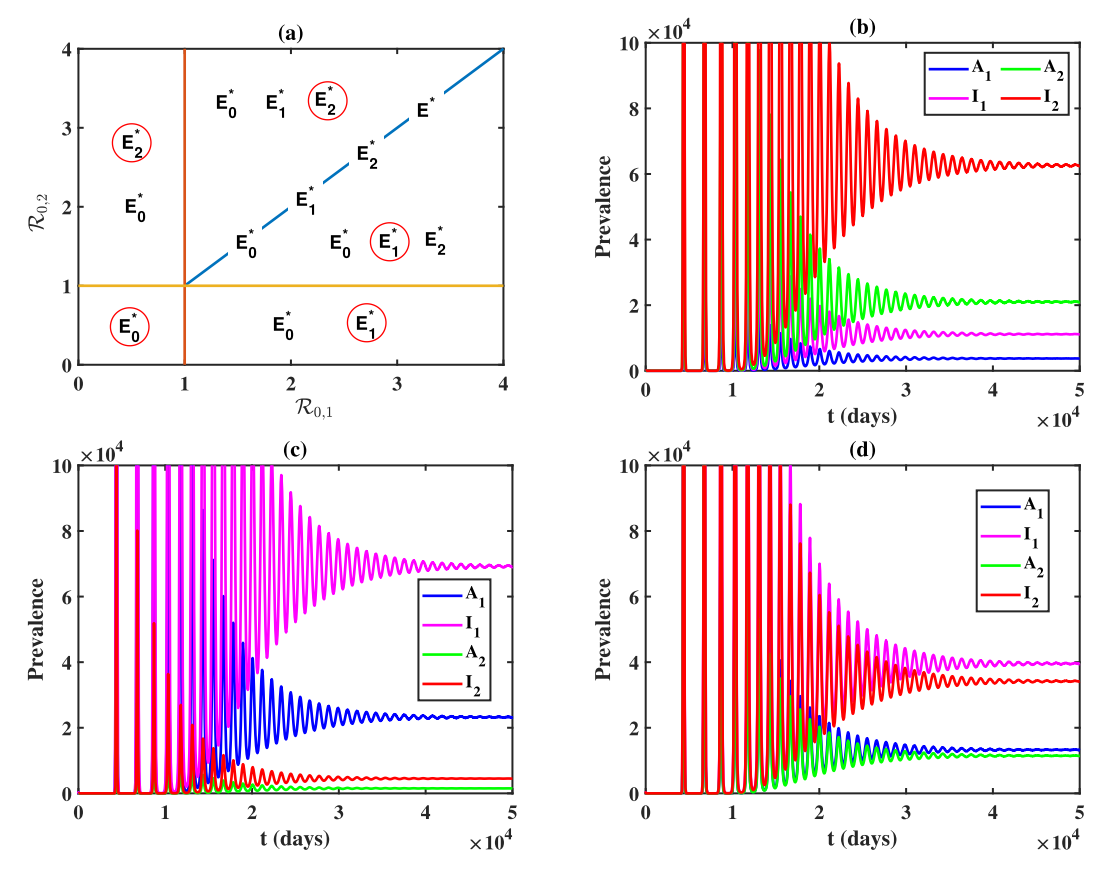
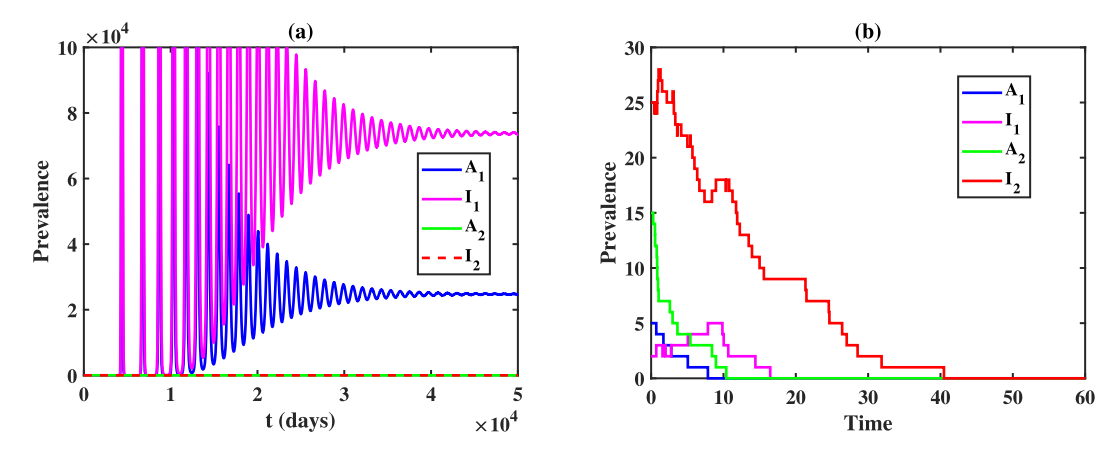


Fig. 3. (a): The existence and stability of the equilibria of model (2) with different values of  $\mathcal{R}_{0,1}$  and  $\mathcal{R}_{0,2}$ . The circled equilibrium is stable in each region. (b-d): The prevalence using the fitted parameter values for strain 1 (see Table 3) and setting parameter values for strain 2 to be the same as strain 1. Hence,  $\mathcal{R}_{0,1} = \mathcal{R}_{0,2} = 11.1505$ . The initial conditions used in (b-d) are  $(S_0, A_{1,0}, I_{1,0}, A_{2,0}, I_{2,0}, R_0) = (1000, 5, 2, 15, 25, 100)$ ,  $(S_0, A_{1,0}, I_{1,0}, A_{2,0}, I_{2,0}, R_0) = (1000, 500, 100, 400, 120, 1000)$ , respectively. They show that there are multiple stable interior equilibrium points when  $\mathcal{R}_{0,1} = \mathcal{R}_{0,2}$ .



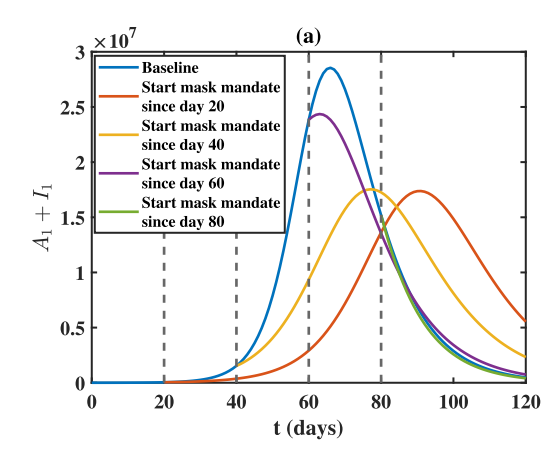
**Fig. 4.** (a): The prevalence using the deterministic model (2). (b): A sample path of the corresponding stochastic model (Table 4). In both panels, the parameter values are from Table 3 with  $\mathcal{R}_{0,1} = 11.1505$  and  $\mathcal{R}_{0,2} = 1.5547$ , and the initial conditions are  $(S_0, A_{1,0}, I_{1,0}, A_{2,0}, I_{2,0}, R_0) = (1000, 5, 2, 15, 25, 100)$ . (a) shows that the strain-1-dominant equilibrium  $E_1^*$  exists and is stable. (b) shows that even though  $\mathcal{R}_{0,1} > 1$  and  $\mathcal{R}_{0,2} > 1$ , the disease may die out within a relatively short period.

# 4.4. Control strategies

From the simulation in the last section, we know that control strategies that reduce the transmission and consequently the basic reproduction number would be important in mitigating the disease spread, especially when the control measures are implemented early. In this section, we use the mask mandate as an example to further study the implementation of control strategies. We introduce two more parameters, e and c, to represent the mask efficacy and mask coverage, respectively. Hence, the transmission rates  $\beta_{A_i}$  and  $\beta_{I_i}$  (i=1,2) are

lowered by multiplying by (1-ec), where both e and c are between 0 and 1. In this case, we have two corresponding control reproduction numbers. We denote them as  $\mathcal{R}_{c,1}$  and  $\mathcal{R}_{c,2}$ , respectively.

We first assume e=40%, c=75% and consider different starting dates of the mask mandate. If it is implemented on day 20, 40, or 60 after the omicron variant appears, the outbreak peak for strain 1 will be lowered and delayed compared with the baseline case in which there is no mask mandate (c=0). In these cases, the mask mandate is initiated before the peak of strain 1. If we start the control on day 80 (after the peak), the prevalence will only be slightly lowered (see Fig. 5(a)).



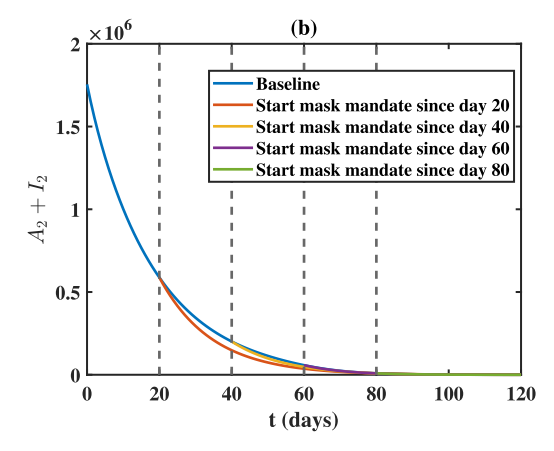


Fig. 5. Prevalence of strain 1 (a) and strain 2 (b) with different starting dates of mask mandate. In all panels we assume the mask efficacy and coverage to be 40% and 75%, respectively. The initial conditions and all the other parameter values are from Table 3. It shows that if we start the mask mandate early (before the infection peak), the peak will be lowered and delayed. However, if we start late (after the peak), the prevalence will only be slightly lowered.

Table 4
A stochastic model corresponding to model (2).

Event	Change	Probability
Infection of strain 1 by A <sub>1</sub>	$(S, A_1, I_1, A_2, I_2, R) \rightarrow (S - 1, A_1 + 1, I_1, A_2, I_2, R)$	$\beta_{A_1} S A_1 \Delta t$
Infection of strain 1 by $I_1$	$(S, A_1, I_1, A_2, I_2, R) \rightarrow (S - 1, A_1 + 1, I_1, A_2, I_2, R)$	$\beta_{I_1} S I_1 \Delta t$
Infection of strain 2 by $A_2$	$(S, A_1, I_1, A_2, I_2, R) \rightarrow (S - 1, A_1, I_1, A_2 + 1, I_2, R)$	$\beta_{A_2} S A_2 \Delta t$
Infection of strain 2 by $I_2$	$(S, A_1, I_1, A_2, I_2, R) \rightarrow (S - 1, A_1, I_1, A_2 + 1, I_2, R)$	$\beta_{I_2} S I_2 \Delta t$
Natural death for S	$(S, A_1, I_1, A_2, I_2, R) \rightarrow (S - 1, A_1, I_1, A_2, I_2, R)$	μ.SΔt
Transition from $A_1$ to $I_1$	$(S, A_1, I_1, A_2, I_2, R) \rightarrow (S, A_1 - 1, I_1 + 1, A_2, I_2, R)$	$\alpha_1 A_1 \Delta t$
Recovery from $A_1$	$(S, A_1, I_1, A_2, I_2, R) \rightarrow (S, A_1 - 1, I_1, A_2, I_2, R + 1)$	$\gamma_{A_1} A_1 \Delta t$
Natural death for $A_1$	$(S, A_1, I_1, A_2, I_2, R) \rightarrow (S, A_1 - 1, I_1, A_2, I_2, R)$	$\mu A_1 \Delta t$
Disease-induced death for $I_1$	$(S, A_1, I_1, A_2, I_2, R) \rightarrow (S, A_1, I_1 - 1, A_2, I_2, R)$	$\omega_1 I_1 \Delta t$
Recovery from $I_1$	$(S, A_1, I_1, A_2, I_2, R) \rightarrow (S, A_1, I_1 - 1, A_2, I_2, R + 1)$	$\gamma_{I_1} I_1 \Delta t$
Natural death for $I_1$	$(S, A_1, I_1, A_2, I_2, R) \rightarrow (S, A_1, I_1 - 1, A_2, I_2, R)$	$\mu \dot{I}_1 \Delta t$
Transition from $A_2$ to $I_2$	$(S, A_1, I_1, A_2, I_2, R) \rightarrow (S, A_1, I_1, A_2 - 1, I_2 + 1, R)$	$\alpha_2 A_2 \Delta t$
Recovery from $A_2$	$(S, A_1, I_1, A_2, I_2, R) \rightarrow (S, A_1, I_1, A_2 - 1, I_2, R + 1)$	$\gamma_{A_2} A_2 \Delta t$
Natural death for $A_2$	$(S, A_1, I_1, A_2, I_2, R) \rightarrow (S, A_1, I_1, A_2 - 1, I_2, R)$	$\mu A_2 \Delta t$
Disease-induced death for $I_2$	$(S, A_1, I_1, A_2, I_2, R) \rightarrow (S, A_1, I_1, A_2, I_2 - 1, R)$	$\omega_2 I_2 \Delta t$
Recovery from $I_2$	$(S, A_1, I_1, A_2, I_2, R) \rightarrow (S, A_1, I_1, A_2, I_2 - 1, R + 1)$	$\gamma_{I_2} I_2 \Delta t$
Natural death for $I_2$	$(S, A_1, I_1, A_2, I_2, R) \rightarrow (S, A_1, I_1, A_2, I_2 - 1, R)$	$\mu I_2 \Delta t$
Natural death for R	$(S, A_1, I_1, A_2, I_2, R) \rightarrow (S, A_1, I_1, A_2, I_2, R - 1)$	$\mu R \Delta t$
Birth	$(S,A_1,I_1,A_2,I_2,R) \to (S+1,A_1,I_1,A_2,I_2,R)$	$\mu N \Delta t$

Similar results are found for strain 2 (see Fig. 5(b)), in which they are after the peak even for the baseline case.

We further study the impact of mask-wearing on the prevalence of strain 1 and strain 2. Fig. 6(a) and (b) are contour maps for the control reproduction numbers  $\mathcal{R}_{c,1}$  and  $\mathcal{R}_{c,2}$  with different mask-wearing strategies. We can see that as the mask coverage and efficacy increase, both  $\mathcal{R}_{c,1}$  and  $\mathcal{R}_{c,2}$  decrease. However, to achieve  $\mathcal{R}_{c,1} < 1$ , we need a high mask efficacy and coverage. For example, if the mask efficacy is as high as 95%, we still need about 95% of the population to wear masks. However, this high percentage of mask-wearing is hard to achieve in practice. It implies that we need more control strategies, such as vaccination, combined with the mask mandate to slow down the spread of COVID-19.

In Fig. 6(c) and (d), we increase the mask efficacy to 70% and consider the prevalence for strain 1 and strain 2 with different mask coverages. As mask coverage increases, the prevalence will be reduced. In addition, the infection peak will be lowered and delayed. Fig. 6(c) also reveals that there will be several subsequent waves. However, we observe a relatively long period with a low infection level between the first and second peaks. One possible reason is that we assume natural immunity to be permanent. If a large portion of the population has been infected and the recruitment rate for susceptible individuals is not high enough, the prevalence will stay at a low level for a while.

The mask mandate will be lifted at some point. We are interested in the impact of the lifting date on the first and subsequent waves. If we focus on a specific case in Fig. 6(c), i.e. c=0.6, the first peak is about  $1.2\times10^7$  on day 140 and there are 3 peaks within the first 10,000 days. Now we consider lifting the mask mandate on different dates and 10% of the population will still wear masks after lifting. The baseline case is no lifting. Fig. 7(a) shows that lifting the mask mandate before the prevalence peak will result in an earlier and much higher first peak. In contrast, lifting after the peak does not influence the prevalence much. In Fig. 7(b) we can see that by lifting the mask mandate we could have at least 4 peaks within the first 10,000 days. Interestingly, among these five cases, the latest lifting leads to the earliest subsequent wave. The reason could be that in this case, we have more susceptible individuals once the mask mandate is lifted. Even though the lifting date affects the time of the subsequent waves, it only has a minor influence on the scale of the subsequent waves. Lifting at any time leads to an earlier peak than that when the mask mandate is always required.

# 5. Conclusion and discussion

In this paper, we developed a multi-strain model with infectious asymptomatic classes and applied it to the COVID-19 dynamics in the US. Starting from a two-strain model, we obtained basic reproduction numbers for the two strains and interpreted their biological meanings. Rigorous analyses for the local and global stability of the DFE were given. We also derived explicit formulas for two strain-dominant equilibria and analyzed their local and global stability. The existence of

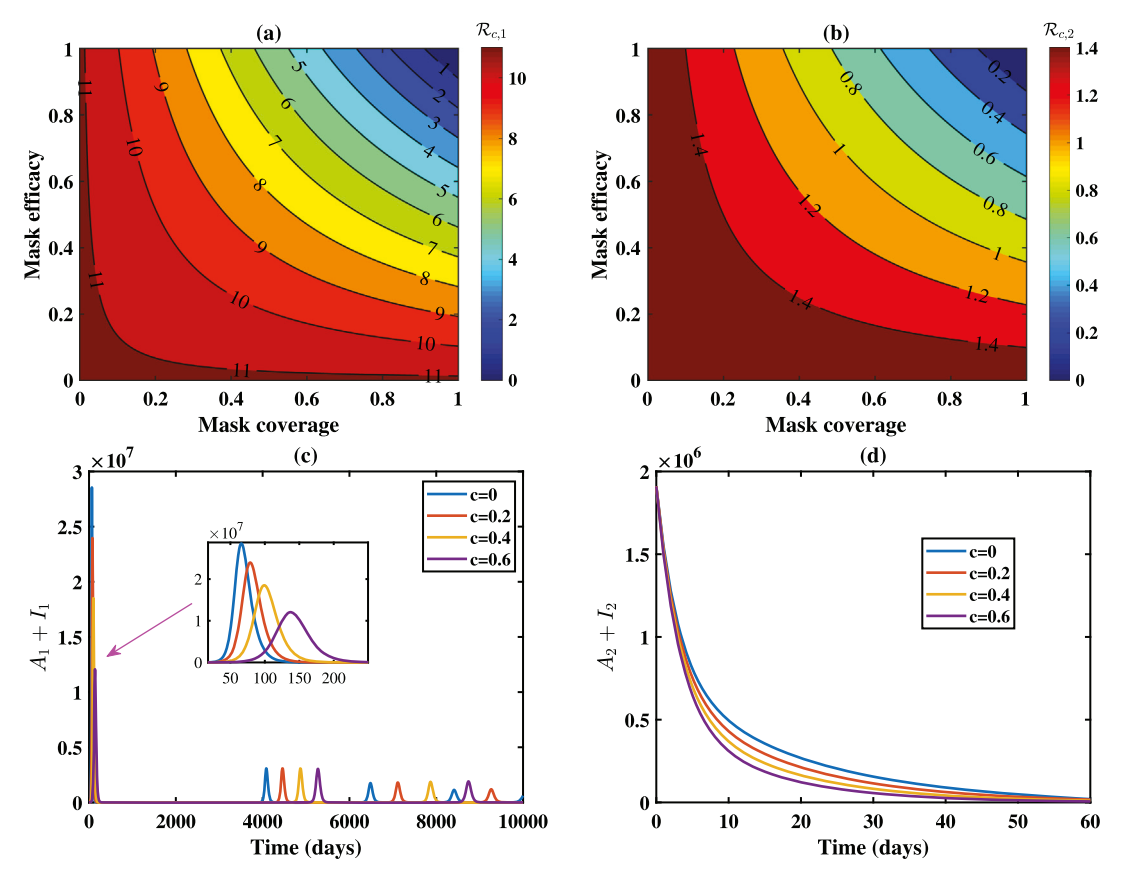


**Fig. 6.** (a–b): Contour maps for the control reproduction numbers  $\mathcal{R}_{c,1}$  and  $\mathcal{R}_{c,2}$  with different mask wearing strategies. (c–d): Prevalence of strain 1 and strain 2 with different mask coverages. In (c) and (d), we assume mask efficacy is 70%. In all panels, the parameter values and initial conditions are from Table 3. (a) and (b) show that as the mask efficacy and coverage increase, both  $\mathcal{R}_{c,1}$  and  $\mathcal{R}_{c,2}$  will decrease. However, to achieve  $\mathcal{R}_{c,1} < 1$ , we need a high mask efficacy and coverage. (c) and (d) show that as mask coverage increases, the prevalence will be reduced. In addition, the infection peak will be lowered and delayed. (c) also reveals that there will be several subsequent waves.

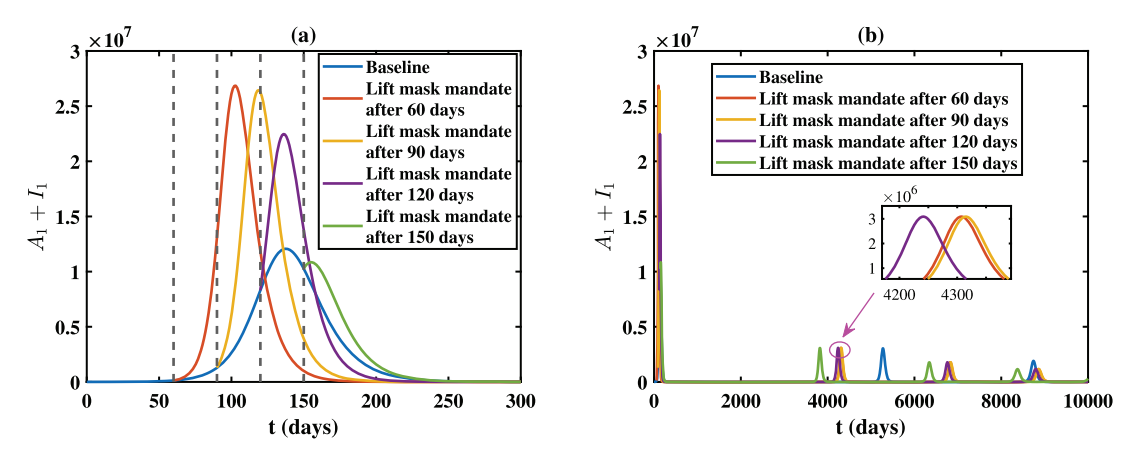


Fig. 7. Prevalence of strain 1 with different lifting dates of mask mandate. In all panels, the mask efficacy is assumed to be 70%; the mask coverage is 60% before lifting and 10% after. The parameter values and initial conditions are from Table 3. (a) shows that lifting the mask mandate before the prevalence peak will result in an earlier and much higher first peak. (b) illustrates the impact of lifting dates on subsequent waves.

the interior equilibrium was also given. Due to the complexity of the model, the stability of the interior or coexistence equilibrium was only numerically investigated. We expanded the analytical results from the two-strain to the *n*-strain case. The analysis shows that only when the basic reproduction numbers for all strains are less than one, the disease is predicted to die out. Otherwise, the strain with the largest reproduction number will persist and the other strains will gradually disappear. In the special case when the reproduction numbers are the same for

all strains, there will be infinitely many interior equilibria. This is reasonable as no strain can invade others. This result implies that the competitive exclusion principle still holds, which has been discussed in other models without infectious asymptomatic classes (Martcheva and Li, 2013; Saucedo and Martcheva, 2017; Dang et al., 2016; Duan et al., 2018; Cai et al., 2013; Rong et al., 2007, 2012). These results were summarized and numerically shown in Figs. 3 and 4(a).

We calibrated model (2) using the data of COVID-19 daily cases and omicron proportions in the US. The fitted parameter values and initial conditions were listed in Table 3. Fitting results with the 95% confidence interval (CI) were shown in Fig. 2. We found that the omicron variants are more transmissible but less fatal from the data fitting. Using the fitted parameter values, we calculated the basic reproduction number for the omicron variants as 11.1505. It is much larger than that for the delta variants, which is 1.5547. Liu et al. also found that the basic reproduction number for the omicron variants is much larger than the other variants (Liu and Rocklöv, 2022). They reviewed several papers and found the average basic reproduction number for the omicron variants is 8.2, which is about 3.8 times that of the original strain. Hibberd reckoned the basic reproduction number for the omicron variants could be as high as 10 (Burki, 2022). However, Khan and Atangana estimated this value to be 2.1107 in South Africa (Khan and Atangana, 2022). Regarding the reproduction number of the delta variants, our result is smaller compared with some other papers. For example, Zhang et al. estimated this value as 3.2 based on the data from China in May 2021 (Zhang et al., 2021). Head et al. estimated it as 4.6 using data from the US in August 2021 (Head et al., 2022). A possible reason for this disparity may be the insufficient data used to estimate the number. In many regions, the COVID-19 case data are underreported. Another reason might be due to the time difference of data sets. The data set chosen in this paper is from 11/24/2021 to 1/12/2022, when the omicron variants emerged and outcompeted the previously circulating delta variants. In addition, different models focus on specific questions without including all possible factors that may affect the estimation.

Using a stochastic model corresponding to the deterministic model, we showed that even when the basic reproduction number is greater than one, the disease could still die out within a short period, especially during the initial stage in which the infected population size is low (see Table 4 and Fig. 4(b)). Similar results were found in Srivastav et al. (2021). They also showed that stochasticity would play an important role in a small population. This implies that it is crucial to implement control strategies early. We used the mask mandate as an example to further address this problem. Fig. 4 showed that the prevalence peak will be lowered and delayed if we start the mask mandate before the peak. However, if we start after the peak, the prevalence will only be slightly reduced. The importance of implementing control strategies early was also demonstrated in some previous papers. In He et al. (2021), we found that to prevent a subsequent wave, timely screening and detection would be needed in the early stage of infection. In Shen et al. (2021b), we showed that there would be more averted infections and deaths if the executive order was implemented earlier. Knock et al. also estimated that the mortality in England could be roughly halved if the lockdown had been introduced one week earlier (Knock et al., 2021).

The lifting date of the mask mandate also affects the dynamics of COVID-19 transmission. Fig. 7(a) showed that lifting the mask mandate before the prevalence peak would result in an earlier and much higher first peak. In contrast, lifting after the peak would not influence the prevalence much. In addition, lifting dates would affect the number and the time of the subsequent waves, but only have minor influences on the scale of the subsequent waves (Fig. 7(b)). Similar results were also shown in Ngonghala et al. (2020). They found that early termination of the social-distancing measures could lead to a devastating second wave with a disease burden similar to the scenario without implementing the social-distancing measures. We also found that choosing the lifting date would be tricky if a large portion of the population still remains susceptible. In a recent study, Sonabend et al. showed that if the timing of non-pharmaceutical interventions (NPIs) could be carefully balanced against the vaccination coverage, the risk of a large subsequent wave of COVID-19 hospitalization resulting from lifting NPIs can be reduced (Sonabend et al., 2021).

In this paper, we adopted the SAIR (susceptible-asymptomatic infected-symptomatic infected-recovered) modeling framework. The asymptomatic and pre-symptomatic individuals are grouped into one class. Because we are more interested in studying the competition between different strains and the impact of the way of implementing control strategies, we used a simple modeling framework and did not consider the exposed class, which was also ignored in some other COVID-19 papers (Massard et al., 2022; Calleri et al., 2021; Serhani and Labbardi, 2021). In view of the observation that the breakthrough infection or reinfection only accounts for a small portion of the total infection, we assumed the acquired immunity to be permanent after recovery, which was also the assumption in many other papers of COVID-19 (Massard et al., 2022; Calleri et al., 2021; Serhani and Labbardi, 2021; Huo et al., 2021; Musa et al., 2022; Shen et al., 2021a,b; Li et al., 2021b). If we add more classes such as the exposed class, the basic reproduction numbers and the dynamics of the model will be slightly different from that obtained using the model in this paper. For example, the prevalence peak will be slightly delayed when including the exposed class. If we use the SAIRS modeling framework by considering waning immunity after recovery, the basic reproduction number will remain the same but the prevalence peak will be earlier and higher.

Although asymptomatic transmission does not affect the competition between different strains, several studies have shown that asymptomatic infection plays an important role in COVID transmission, and that implementing control strategies targeting asymptomatic infected individuals is critical. For example, Lovell-Read et al. found that interventions targeting asymptomatic cases are important to prevent local outbreaks (Lovell-Read et al., 2021). Hart et al. showed the importance of continued contact tracing because of COVID's high infectiousness immediately prior to symptom onset (Hart et al., 2021). The focus of this paper is to study the competition between different strains and the influence of the ways of implementing control strategies. For simplicity of modeling, we did not include control strategies specifically targeting asymptomatic individuals. In addition, parameter identifiability analysis is important in data fitting and parameter estimation. It is used to describe whether it is possible to uniquely recover model parameters from a given set of data. Structural identifiability analysis is usually performed first, followed by practical identifiability analysis. A rigorous analysis can be challenging, if not impossible, for models involving many variables and parameters with only limited data available. Here we did not intend to obtain accurate estimates of model parameters in view of the model complexity and the available data. Instead, we fixed some parameters from the literature and allowed a few to vary to see if the model prediction can quantitatively capture (at least the trend of) the available data.

In summary, we developed a multi-strain model with infectious asymptomatic individuals to investigate the transmission of COVID-19. Even though the data used here are from the US and we used the mask mandate as an example of control measures, the analytical and numerical results could be applied to other regions and other control strategies. The results may help better understand the transmission dynamics between different strains and provide useful information for policymakers to formulate guidelines of control strategies (Hart et al., 2021; Lovell-Read et al., 2021).

# CRediT authorship contribution statement

Shasha Gao: Conceptualization, Methodology, Formal analysis, Writing – original draft. Mingwang Shen: Methodology, Writing – original draft. Xueying Wang: Conceptualization, Methodology, Formal analysis, Writing – original draft. Jin Wang: Conceptualization, Methodology, Writing – review & editing. Maia Martcheva: Methodology, Writing – review & editing. Libin Rong: Conceptualization, Methodology, Writing – original draft, Writing – review & editing, Supervision.

#### **Declaration of competing interest**

The authors declare that they have no known competing financial interests or personal relationships that could have appeared to influence the work reported in this paper.

#### Acknowledgments

M. Shen is supported by the National Natural Science Foundation of China (12171387), China Postdoctoral Science Foundation (2018M631134 and 2020T130095ZX), and the Young Talent Support Program of Shaanxi University Association for Science and Technology (20210307). X. Wang's research is partially supported by a grant from the Simons Foundation (960466). J. Wang is supported by the NSF Grant DMS-1951345 and DMS-1913180. M. Martcheva is supported by the NSF grant DMS-1951595. L. Rong is supported by the NSF Grant DMS-1950254.

# Appendix A. Basic reproduction number and the proof of Theorem $\boldsymbol{1}$

Reordering variables as  $x=(A_1,I_1,A_2,I_2,S,R)$ , we get the DFE of system (2)  $E_0^*=(0,0,0,0,S_0^*,0)$ , where  $S_0^*=\frac{A}{\mu}$ . We rewrite system (2) as  $\dot{x}=\mathcal{F}(x)-\mathcal{V}(x)$ , where

$$\mathcal{F} = \begin{pmatrix} \lambda_1 S \\ 0 \\ \lambda_2 S \\ 0 \\ 0 \\ 0 \end{pmatrix}, \qquad \mathcal{V} = \begin{pmatrix} \delta_{A_1} A_1 \\ -\alpha_1 A_1 + \delta_{I_1} I_1 \\ \delta_{A_2} A_2 \\ -\alpha_2 A_2 + \delta_{I_2} I_2 \\ -A + S \sum_{i=1}^2 \lambda_i + \mu S \\ -\sum_{i=1}^2 (\gamma_{A_i} A_i + \gamma_{I_i} I_i) + \mu R \end{pmatrix},$$

with  $\lambda_i = \beta_{A_i} A_i + \beta_{I_i} I_i$ , i = 1,2. According to Van den Driessche and Watmough (2002), we have to check the hypotheses A(1)-A(5). The first four hypotheses are easy to verify. A(5) will be satisfied if all eigenvalues of the matrix

$$J = \begin{pmatrix} -V & 0 \\ J_3 & J_4 \end{pmatrix}$$

have negative real parts. Here

$$V = \begin{pmatrix} \delta_{A_1} & 0 & 0 & 0 \\ -\alpha_1 & \delta_{I_1} & 0 & 0 \\ 0 & 0 & \delta_{A_2} & 0 \\ 0 & 0 & -\alpha_2 & \delta_{I_2} \end{pmatrix}, \qquad J_4 = \begin{pmatrix} -\mu & 0 \\ 0 & -\mu \end{pmatrix},$$

and  $J_3$  is a 2  $\times$  4 matrix. Hence the hypothesis A(5) is satisfied. Taking the Jacobian matrices of  $\mathcal F$  and  $\mathcal V$  around the  $E_0^*$ , we get

$$D\mathcal{F}(E_0^*) = \begin{pmatrix} F & 0 \\ 0 & 0 \end{pmatrix}, \qquad D\mathcal{V}(E_0^*) = \begin{pmatrix} V & 0 \\ J_3 & J_4 \end{pmatrix},$$

where

$$F = \begin{pmatrix} S_0^*\beta_{A_1} & S_0^*\beta_{I_1} & 0 & 0 \\ 0 & 0 & 0 & 0 \\ 0 & 0 & S_0^*\beta_{A_2} & S_0^*\beta_{I_2} \\ 0 & 0 & 0 & 0 \end{pmatrix},$$

 ${\cal V},\,{\cal J}_3$  and  ${\cal J}_4$  are the same as above. We have

$$FV^{-1} = \begin{pmatrix} a_{11} & a_{12} & 0 & 0 \\ 0 & 0 & 0 & 0 \\ 0 & 0 & a_{33} & a_{34} \\ 0 & 0 & 0 & 0 \end{pmatrix},$$

where

$$\begin{split} a_{11} &= \frac{\Lambda \beta_{A_1}}{\mu \delta_{A_1}} + \frac{\Lambda \alpha_1 \beta_{I_1}}{\mu \delta_{A_1} \delta_{I_1}}, \qquad a_{12} = \frac{\lambda \beta_{I_1}}{\mu \delta_{I_1}}, \\ a_{33} &= \frac{\Lambda \beta_{A_2}}{\mu \delta_{A_2}} + \frac{\Lambda \alpha_2 \beta_{I_2}}{\mu \delta_{A_2} \delta_{I_2}}, \qquad a_{34} = \frac{\lambda \beta_{I_2}}{\mu \delta_{I_2}}. \end{split}$$

We denote  $a_{11}$ ,  $a_{33}$  by  $\mathcal{R}_{0.1}$  and  $\mathcal{R}_{0.2}$ , respectively. It follows that

$$\mathcal{R}_0 = \rho(FV^{-1}) = \max\{\mathcal{R}_{0,1}, \mathcal{R}_{0,2}\},\$$

where  $\rho(A)$  denotes the spectral radius of the matrix A.

Since  $\mathcal{R}_0$  is derived using the next generation matrix method, by Theorem 2 in Van den Driessche and Watmough (2002),  $E_0^*$  is locally asymptotically stable when  $\mathcal{R}_0 < 1$  (i.e.  $\mathcal{R}_{0,1} < 1$  and  $\mathcal{R}_{0,2} < 1$ ), and unstable when  $\mathcal{R}_0 > 1$  (i.e.  $\mathcal{R}_{0,1} > 1$  or  $\mathcal{R}_{0,2} < 1$ ).

# Appendix B. Proof of Theorem 2

We define the following Lyapunov function

$$L_1 = S - S_0^* - S_0^* \ln \frac{S}{S_0^*} + A_1 + A_2 + \sum_{i=1}^2 \frac{S_0^* \beta_{I_i}}{\delta_{I_i}} I_{i}.$$

It is clear that  $L_1$  is radially unbounded and positive definite in the entire space  $\Omega$ . The derivative of  $L_1$  along the trajectories of system (2) yields

$$\begin{split} \dot{L_1} = & \left(1 - \frac{S_0^*}{S}\right) S' + \sum_{i=1}^2 A_i' + \sum_{i=1}^2 \frac{S_0^* \beta_{I_i}}{\delta_{I_i}} I_i' \\ = & \left(1 - \frac{S_0^*}{S}\right) \left[\Lambda - S \sum_{i=1}^2 (\beta_{A_i} A_i + \beta_{I_i} I_i) - \mu S\right] \\ & + \sum_{i=1}^2 \left[S(\beta_{A_i} A_i + \beta_{I_i} I_i) - \delta_{A_i} A_i\right] \\ & + \sum_{i=1}^2 \frac{S_0^* \beta_{I_i}}{\delta_{I_i}} (\alpha_i A_i - \delta_{I_i} I_i). \end{split}$$

Using the equilibrium equation  $\Lambda = \mu S_0^*$ , we get

$$\begin{split} \dot{L}_1 &= -\frac{\mu}{S}(S - S_0^*)^2 + S_0^* \sum_{i=1}^2 (\beta_{A_i} A_i + \beta_{I_i} I_i) \\ &- \sum_{i=1}^2 \delta_{A_i} A_i + \sum_{i=1}^2 \frac{S_0^* \beta_{I_i}}{\delta_{I_i}} (\alpha_i A_i - \delta_{I_i} I_i) \\ &= -\frac{\mu}{S}(S - S_0^*)^2 + \delta_{A_1} (\mathcal{R}_{0,1} - 1) A_1 + \delta_{A_2} (\mathcal{R}_{0,2} - 1) A_2 \end{split}$$

When  $\mathcal{R}_0 \leq 1$ , we have  $\mathcal{R}_{0,1} \leq 1$  and  $\mathcal{R}_{0,2} \leq 1$ . Then  $L_1 \leq 0$  and the only potential point for  $L_1 = 0$  is at the DFE. Therefore, by Krasovkii-LaSalle Theorem Martcheva (2015), the DFE  $E_0^*$  is globally asymptotically stable when  $\mathcal{R}_0 \leq 1$ .

# Appendix C. Proof of Theorem 3

We first consider the strain-1-dominant equilibrium, in which both  $A_2$  and  $I_2$  are zero. Setting the right hand side of the system (2) to zero, we have

$$\begin{cases} 0 = \Lambda - S(\beta_{A_1} A_1 + \beta_{I_1} I_1) - \mu S, \\ 0 = S(\beta_{A_1} A_1 + \beta_{I_1} I_1) - \delta_{A_1} A_1, \\ 0 = \alpha_1 A_1 - \delta_{I_1} I_1, \\ 0 = \gamma_{A_1} A_1 + \gamma_{I_1} I_1 - \mu R. \end{cases}$$
(C.1)

From the third equation of (C.1), we get

$$I_1 = \frac{\alpha_1}{\delta_L} A_1.$$

Substituting it into the last and second equation of (C.1), we get

$$R = \frac{1}{\mu} \left( \gamma_{A_1} + \gamma_{I_1} \frac{\alpha_1}{\delta_{I_1}} \right) A_1,$$

and

$$S\bigg(\beta_{A_1}A_1+\beta_{I_1}\frac{\alpha_1}{\delta_{I_1}}A_1\bigg)-\delta_{A_1}A_1=0.$$

Since at strain-1-dominant equilibrium,  $A_1 \neq 0$ , we get

$$S = \frac{\delta_{A_1}}{\beta_{A_1} + \beta_{I_1} \frac{\alpha_1}{\delta_{I_1}}} = \frac{1}{\frac{\beta_{A_1}}{\delta_{A_1}} + \frac{\beta_{I_1} \alpha_1}{\delta_{A_1} \delta_{I_1}}} = \frac{\Lambda}{\mu} \frac{1}{\mathcal{R}_{0,1}}.$$

Adding the first and second equations of (C.1), we get

$$\Lambda - \mu S - \delta_{A_1} A_1 = 0.$$

Hence,

$$A_1 = \frac{\mu}{\delta_{A_1}} \left( \frac{\Lambda}{\mu} - S \right) = \frac{\Lambda}{\delta_{A_1}} \left( 1 - \frac{1}{\mathcal{R}_{0,1}} \right).$$

Therefore, when  $\mathcal{R}_{0,1}>1$ , we have a unique strain-1-dominant equilibrium  $E_1^*=(S_1^*,A_1^*,I_1^*,0,0,R_1^*)$ , where

$$\begin{split} S_1^* &= \frac{\varLambda}{\mu} \frac{1}{\mathcal{R}_{0,1}}, \qquad A_1^* &= \frac{\varLambda}{\delta_{A_1}} \bigg( 1 - \frac{1}{\mathcal{R}_{0,1}} \bigg), \\ I_1^* &= \frac{\alpha_1}{\delta_{I_1}} A_1^*, \qquad R_1^* &= \frac{1}{\mu} \bigg( \gamma_{A_1} + \gamma_{I_1} \frac{\alpha_1}{\delta_{I_1}} \bigg) A_1^*. \end{split}$$

Similarly, when  $\mathcal{R}_{0,2}>1$ , we have a unique strain-2-dominant equilibrium  $E_2^*=(S_2^*,0,0,A_2^*,I_2^*,R_2^*)$ , where

$$\begin{split} S_2^* &= \frac{\varLambda}{\mu} \frac{1}{\mathcal{R}_{0,2}}, \qquad A_2^* &= \frac{\varLambda}{\delta_{A_2}} \bigg( 1 - \frac{1}{\mathcal{R}_{0,2}} \bigg), \\ I_2^* &= \frac{\alpha_2}{\delta_{I_2}} A_{2,2}^*, \qquad R_2^* &= \frac{1}{\mu} \bigg( \gamma_{A_2} + \gamma_{I_2} \frac{\alpha_2}{\delta_{I_2}} \bigg) A_2^* \end{split}$$

# Appendix D. Proof of Theorem 4

The Jacobian matrix of the system (2) (reorder variables as  $x = (A_1, I_1, A_2, I_2, S, R)^T$ ) evaluated at the strain-1-dominant equilibrium  $E_1^*$  is

$$J(E_1^*) = \begin{pmatrix} a_{11} & S_1^*\beta_{I_1} & 0 & 0 & a_{15} & 0 \\ \alpha_1 & a_{22} & 0 & 0 & 0 & 0 \\ 0 & 0 & a_{33} & S_1^*\beta_{I_2} & 0 & 0 \\ 0 & 0 & \alpha_2 & a_{44} & 0 & 0 \\ -S_1^*\beta_{A_1} & -S_1^*\beta_{I_1} & -S_1^*\beta_{A_2} & -S_1^*\beta_{I_2} & a_{55} & 0 \\ \gamma_{A_1} & \gamma_{I_1} & 0 & 0 & 0 & -\mu \end{pmatrix},$$

where

$$\begin{split} a_{11} &= S_1^* \beta_{A_1} - \delta_{A_1}, \qquad a_{15} &= \beta_{A_1} A_1^* + \beta_{I_1} I_1^*, \qquad a_{22} = -\delta_{I_1}, \\ a_{33} &= S_1^* \beta_{A_2} - \delta_{A_2}, \qquad a_{44} = -\delta_{I_2}, \qquad a_{55} = -(\beta_{A_1} A_1^* + \beta_{I_1} I_1^*) - \mu. \end{split}$$

One eigenvalue is  $-\mu$  and the others satisfy

$$\begin{vmatrix} \lambda - a_{11} & -S_1^* \beta_{I_1} & 0 & 0 & -a_{15} \\ -\alpha_1 & \lambda - a_{22} & 0 & 0 & 0 \\ 0 & 0 & \lambda - a_{33} & -S_1^* \beta_{I_2} & 0 \\ 0 & 0 & -\alpha_2 & \lambda - a_{44} & 0 \\ S_1^* \beta_{A_1} & S_1^* \beta_{I_1} & S_1^* \beta_{A_2} & S_1^* \beta_{I_2} & \lambda - a_{55} \end{vmatrix} = 0.$$

Adding the first row to the last row, we get

$$\left| \begin{array}{cccccc} \lambda - a_{11} & -S_1^*\beta_{I_1} & 0 & 0 & -a_{15} \\ -\alpha_1 & \lambda - a_{22} & 0 & 0 & 0 \\ 0 & 0 & \lambda - a_{33} & -S_1^*\beta_{I_2} & 0 \\ 0 & 0 & -\alpha_2 & \lambda - a_{44} & 0 \\ \lambda + \delta_{A_1} & 0 & S_1^*\beta_{A_2} & S_1^*\beta_{I_2} & \lambda + \mu \end{array} \right| = 0.$$

Expanding along the last column, we get

$$(\lambda + \mu)D_1 - a_{15}D_2 = 0,$$

where  $D_1 = D_3 D_4$  with

$$D_3 = \left| \begin{array}{ccc} \lambda - a_{11} & -S_1^* \beta_{I_1} \\ -\alpha_1 & \lambda - a_{22} \end{array} \right|, \qquad D_4 = \left| \begin{array}{ccc} \lambda - a_{33} & -S_1^* \beta_{I_2} \\ -\alpha_2 & \lambda - a_{44} \end{array} \right|,$$

and  $D_2 = -(\lambda - a_{22})(\lambda + \delta_{A_1})D_4$ . Hence,

$$D_4 \Big[ (\lambda + \mu) D_3 + a_{15} (\lambda - a_{22}) (\lambda + \delta_{A_1}) \Big] = 0.$$

Therefore, three eigenvalues satisfy

$$(\lambda + \mu)D_3 + a_{15}(\lambda - a_{22})(\lambda + \delta_{A_1}) = 0.$$

Using  $D_3$ ,  $a_{15}$  and  $a_{22}$ , we get

$$\begin{split} (\lambda + \mu) \Big[ (\lambda - S_1^* \beta_{A_1} + \delta_{A_1}) (\lambda + \delta_{I_1}) - \alpha_1 S_1^* \beta_{I_1} \Big] \\ + (\beta_{A_1} A_1^* + \beta_{I_1} I_1^*) (\lambda + \delta_{I_1}) (\lambda + \delta_{A_1}) = 0. \end{split}$$

Collecting terms, we have

$$\lambda^3 + a_1 \lambda^2 + a_2 \lambda + a_3 = 0,$$

where

$$\begin{split} a_1 = & \delta_{A_1} - S_1^* \beta_{A_1} + \delta_{I_1} + \mu + (\beta_{A_1} A_1^* + \beta_{I_1} I_1^*), \\ a_2 = & (\delta_{A_1} - S_1^* \beta_{A_1}) \delta_{I_1} - \alpha_1 S_1^* \beta_{I_1} + \mu (\delta_{A_1} - S_1^* \beta_{A_1} + \delta_{I_1}) \\ & + (\beta_{A_1} A_1^* + \beta_{I_1} I_1^*) (\delta_{I_1} + \delta_{A_1}), \\ a_3 = & \mu \Big[ (\delta_{A_1} - S_1^* \beta_{A_1}) \delta_{I_1} - \alpha_1 S_1^* \beta_{I_1} \Big] + (\beta_{A_1} A_1^* + \beta_{I_1} I_1^*) \delta_{I_1} \delta_{A_1}. \end{split}$$

Using the equilibrium condition

$$S_1^*(\beta_{A_1}A_1^*+\beta_{I_1}I_1^*)=\delta_{A_1}A_1^*, \qquad \alpha_1A_1^*=\delta_{I_1}I_1^*,$$

we get

$$\delta_{A_1} - S_1^* \beta_{A_1} = \frac{S_1^* \beta_{I_1} I_1^*}{A_1^*} > 0$$

and

$$(\delta_{A_1} - S_1^*\beta_{A_1})\delta_{I_1} - \alpha_1 S_1^*\beta_{I_1} = \frac{S_1^*\beta_{I_1}I_1^*}{A_1^*}\delta_{I_1} - \alpha_1 S_1^*\beta_{I_1} = \alpha_1 S_1^*\beta_{I_1} - \alpha_1 S_1^*\beta_{I_1} = 0.$$

Therefore,  $a_1>0$ ,  $a_2>0$  and  $a_3>0$ . In addition,  $a_1>\delta_{I_1}$  and  $a_2>(\beta_{A_1}A_1^*+\beta_{I_1}I_1^*)\delta_{A_1}$ . Thus,

$$a_1 a_2 - a_3 > \delta_{I_1} (\beta_{A_1} A_1^* + \beta_{I_1} I_1^*) \delta_{A_1} - a_3 = 0.$$

According to the Routh–Hurwitz criterion, these three eigenvalues all have negative real parts. The other two eigenvalues satisfy  $D_4=0$ . It follows that

$$\lambda^2 + b\lambda + c = 0.$$

where

$$\begin{split} b &= \delta_{A_2} - S_1^* \beta_{A_2} + \delta_{I_2}, \\ c &= (\delta_{A_2} - S_1^* \beta_{A_2}) \delta_{I_2} - \alpha_2 S_1^* \beta_{I_2} = \delta_{A_2} \delta_{I_2} \bigg( 1 - S_1^* \frac{\mu}{A} R_{0,2} \bigg) = \delta_{A_2} \delta_{I_2} \bigg( 1 - \frac{R_{0,2}}{R_{0,1}} \bigg). \end{split}$$

When  $\mathcal{R}_{0,2} < \mathcal{R}_{0,1}$ , we have c > 0. To determine the sign for b, recall that  $S_1^* = \frac{\Lambda}{\mu} \frac{1}{R_{0,1}}$ . Then

$$\begin{split} \mathcal{R}_{0,2} < \mathcal{R}_{0,1} &\Leftrightarrow \mathcal{R}_{0,2} \frac{\mu}{A} S_1^* < 1 \Leftrightarrow S_1^* (\beta_{A_2} \delta_{I_2} + \beta_{I_2} \alpha_2) < \delta_{A_2} \delta_{I_2} \\ &\Rightarrow S_1^* \beta_{A_2} \delta_{I_2} < \delta_{A_2} \delta_{I_2}. \end{split}$$

It follows that  $S_1^*\beta_{A_2} < \delta_{A_2}$ . Hence, b>0. Therefore, when  $\mathcal{R}_{0,1} > \mathcal{R}_{0,2}$ , these two eigenvalues have negative real parts. We can also see that when  $\mathcal{R}_{0,2} > \mathcal{R}_{0,1}$ , we have c<0, which implies that at least one eigenvalue is positive. Therefore, in the case of  $\mathcal{R}_{0,1} > 1$ , when  $\mathcal{R}_{0,1} > \mathcal{R}_{0,2}$ , the strain-1-dominant equilibrium  $E_1^*$  is locally asymptotically stable; when  $\mathcal{R}_{0,1} < \mathcal{R}_{0,2}$ ,  $E_1^*$  is unstable. Similarly, in the case of  $\mathcal{R}_{0,2} > 1$ , when  $\mathcal{R}_{0,2} > \mathcal{R}_{0,1}$ , the strain-2-dominant equilibrium  $E_2^*$  is locally asymptotically stable; when  $\mathcal{R}_{0,2} < \mathcal{R}_{0,1}$ ,  $E_2^*$  is unstable.

#### Appendix E. Proof of Theorem 5

Assuming  $\mathcal{R}_{0,1} > 1$  and  $\mathcal{R}_{0,1} > \mathcal{R}_{0,2}$ , we first consider the strain-1-dominant equilibrium. We define the following Lyapunov function

$$L_2 = \int_{S_1^*}^S \frac{x - S_1^*}{x} dx + \int_{A_1^*}^{A_1} \frac{x - A_1^*}{x} dx + c_1 \int_{I_1^*}^{I_1} \frac{x - I_1^*}{x} dx + A_2 + kc_2 I_2,$$

where  $k = \frac{\delta_{A_2}}{a_2}$ , and  $c_1$  and  $c_2$  are positive constants to be determined later.

It is clear that  $L_2$  is radially unbounded and positive definite in the entire space  $\Omega$ . Differentiating  $L_2$  along solutions of system (2), we have

$$\begin{split} \dot{L_{2}} &= \frac{S - S_{1}^{*}}{S} S' + \frac{A_{1} - A_{1}^{*}}{A_{1}} A'_{1} + c_{1} \frac{I_{1} - I_{1}^{*}}{I_{1}} I'_{1} + A'_{2} + kc_{2} I'_{2} \\ &= \left(1 - \frac{S_{1}^{*}}{S}\right) \left(\Lambda - S \sum_{i=1}^{2} \left(\beta_{A_{i}} A_{i} + \beta_{I_{i}} I_{i}\right) - \mu S\right) \\ &+ \left(1 - \frac{A_{1}^{*}}{A_{1}}\right) \left[S(\beta_{A_{1}} A_{1} + \beta_{I_{1}} I_{1}) - \delta_{A_{1}} A_{1}\right] + c_{1} \left(1 - \frac{I_{1}^{*}}{I_{1}}\right) \left(\alpha_{1} A_{1} - \delta_{I_{1}} I_{1}\right) \\ &+ S \left(\beta_{A_{1}} A_{2} + \beta_{I_{1}} I_{2}\right) - \delta_{A_{2}} A_{2} + kc_{2} \left(\alpha_{2} A_{2} - \delta_{I_{1}} I_{2}\right). \end{split}$$

Using the equilibrium equations

$$\Lambda = S_1^*(\beta_{A_1}A_1^* + \beta_{I_1}I_1^*) + \mu S_1^*, \quad \delta_{A_1} = \frac{S_1^*(\beta_{A_1}A_1^* + \beta_{I_1}I_1^*)}{A_1^*}, \quad \delta_{I_1} = \frac{\alpha_1 A_1^*}{I_1^*},$$

we get

$$\begin{split} \dot{L_2} &= -\mu S \left(1 - \frac{S_1^*}{S}\right)^2 + \left(1 - \frac{S_1^*}{S}\right) \\ &\times \left[S_1^* \left(\beta_{A_1} A_1^* + \beta_{I_1} I_1^*\right) - S \sum_{i=1}^2 \left(\beta_{A_i} A_i + \beta_{I_i} I_i\right)\right] \\ &+ \left(1 - \frac{A_1^*}{A_1}\right) \left[S \left(\beta_{A_1} A_1 + \beta_{I_1} I_1\right) - \frac{S_1^* \left(\beta_{A_1} A_1^* + \beta_{I_1} I_1^*\right)}{A_1^*} A_1\right] \\ &+ c_1 \left(1 - \frac{I_1^*}{I_1}\right) \left(\alpha_1 A_1 - \frac{\alpha_1 A_1^*}{I_1^*} I_1\right) \\ &+ S \left(\beta_{A_2} A_2 + \beta_{I_2} I_2\right) - \delta_{A_2} A_2 + k c_2 \left(\alpha_2 A_2 - \delta_{I_2} I_2\right) \\ &= -\mu S \left(1 - \frac{S_1^*}{S}\right)^2 + \beta_{A_1} S_1^* A_1^* \left(2 - \frac{S_1^*}{S} - \frac{S}{S_1^*}\right) \\ &+ \beta_{I_1} S_1^* I_1^* \left(2 - \frac{S_1^*}{S} + \frac{I_1}{I_1^*} - \frac{A_1}{A_1^*} - \frac{S I_1 A_1^*}{S_1^* I_1^* A_1}\right) \\ &+ c_1 \alpha_1 A_1^* \left(\frac{A_1}{A_1^*} - \frac{I_1}{I_1^*} - \frac{I_1^* A_1}{I_1 A_1^*} + 1\right) \\ &+ \delta_{A_2} A_2 \left(S_1^* \frac{\beta_{A_2}}{\delta_{A_2}} + c_2 - 1\right) + k \delta_{I_2} I_2 \left(S_1^* \frac{\beta_{I_2} \alpha_2}{\delta_{A_2} \delta_{I_2}} - c_2\right). \end{split}$$

Since  $x - 1 \ge \ln x$  for x > 0, we get

$$2 - \frac{S_1^*}{S} - \frac{S_1 I_1 A_1^*}{S_1^* I_1^* A_1} \le -\ln \frac{S_1^*}{S} - \ln \frac{S I_1 A_1^*}{S_1^* I_1^* A_1} = \ln \frac{I_1^*}{I_1} + \ln \frac{A_1}{A_1^*}$$

and

$$1 - \frac{I_1^* A_1}{I_1 A_1^*} \le \ln(\frac{I_1}{I_1^*}) + \ln(\frac{A_1^*}{A_1}).$$

It follows that

$$\begin{split} \dot{L_2} &\leq - \, \mu S \left( 1 - \frac{S_1^*}{S} \right)^2 + \beta_{A_1} S_1^* A_1^* \left( 2 - \frac{S_1^*}{S} - \frac{S}{S_1^*} \right) \\ &+ \left( \beta_{I_1} S_1^* I_1^* - c_1 \alpha_1 A_1^* \right) \left[ \left( \frac{I_1}{I_1^*} - \ln \frac{I_1}{I_1^*} \right) - \left( \frac{A_1}{A_1^*} - \ln \frac{A_1}{A_1^*} \right) \right] \\ &+ \delta_{A_2} A_2 \left( \frac{\mathcal{R}_{0,2}^A}{\mathcal{R}_{0,1}} + c_2 - 1 \right) + k \delta_{I_2} I_2 \left( \frac{\mathcal{R}_{0,2}^I}{\mathcal{R}_{0,1}} - c_2 \right). \end{split}$$

By the arithmetic-geometric mean inequality, we have

$$\frac{S_1^*}{S} + \frac{S}{S^*} \ge 2.$$

Choosing 
$$c_1 = \frac{\beta_{I_1} S_1^* I_1^*}{\alpha_1 A_1^*}$$
 and  $c_2 = \frac{R_{0,2}^I}{R_{0,1}}$ , we get

$$\frac{\mathcal{R}_{0,2}^A}{\mathcal{R}_{0,1}} + c_2 - 1 = \frac{\mathcal{R}_{0,2}}{\mathcal{R}_{0,1}} - 1 < 0.$$

Therefore,  $L_2 \leq 0$ . It is easy to check that  $L_2 = 0$  if and only if the system is at  $E_1^*$ . By Krasovkii-LaSalle Theorem Martcheva (2015),  $E_1^*$  is globally asymptotically stable when  $\mathcal{R}_{0,1} > \max\{1, \mathcal{R}_{0,2}\}$ . By a similar proof,  $E_2^*$  is globally asymptotically stable when  $\mathcal{R}_{0,2} > \max\{1, \mathcal{R}_{0,1}\}$ .

# Appendix F. Proof of Theorem 6

Setting the right-hand side of system (2) to zero, we have

$$\begin{cases} 0 = A - S \sum_{i=1}^{2} (\beta_{A_{i}} A_{i} + \beta_{I_{i}} I_{i}) - \mu S, \\ 0 = S(\beta_{A_{1}} A_{1} + \beta_{I_{1}} I_{1}) - \delta_{A_{1}} A_{1}, \\ 0 = \alpha_{1} A_{1} - \delta_{I_{1}} I_{1}, \\ 0 = S(\beta_{A_{2}} A_{2} + \beta_{I_{2}} I_{2}) - \delta_{A_{2}} A_{2}, \\ 0 = \alpha_{2} A_{2} - \delta_{I_{2}} I_{2}, \\ 0 = \gamma_{A_{1}} A_{1} + \gamma_{I_{1}} I_{1} + \gamma_{A_{2}} A_{2} + \gamma_{I_{2}} I_{2} - \mu R. \end{cases}$$
(F.1)

From the third and fifth equations of (F.1), we get

$$I_1 = \frac{\alpha_1}{\delta_{I_1}} A_1, \qquad I_2 = \frac{\alpha_2}{\delta_{I_2}} A_2.$$

Substituting them into the last equation of (F.1), we get

$$R = \frac{1}{\mu} \left( \gamma_{A_1} + \gamma_{I_1} \frac{\alpha_1}{\delta_{I_1}} \right) A_1 + \frac{1}{\mu} \left( \gamma_{A_2} + \gamma_{I_2} \frac{\alpha_2}{\delta_{I_2}} \right) A_2$$

Replacing  $I_1$  in the second equation of (F.1), we have

$$S\left(\beta_{A_1}A_1 + \beta_{I_1} \frac{\alpha_1}{\delta_{I_1}} A_1\right) - \delta_{A_1}A_1 = 0.$$

At an interior equilibrium,  $A_1 \neq 0$ , we get

$$S = \frac{\delta_{A_1}}{\beta_{A_1} + \beta_{I_1} \frac{\alpha_1}{\delta_{I_1}}} = \frac{\Lambda}{\mu} \frac{1}{\mathcal{R}_{0,1}}.$$

Similarly, from the fourth equation of (F.1), we have

$$S = \frac{\Lambda}{\mu} \frac{1}{\mathcal{R}_{0,2}}.$$

Since  $\mathcal{R}_{0,1}=\mathcal{R}_{0,2}$ , the above results are valid and  $S^*=\frac{\Lambda}{\mu}\frac{1}{\mathcal{R}_{0,1}}$ . It is possible to have an interior equilibrium only when  $\mathcal{R}_{0,1}>1$ . Because  $I_1$ ,  $I_2$  and R can be written in terms of  $A_1$  and  $A_2$ , we only need to solve for  $A_1$  and  $A_2$ . Adding the first, second, and fourth equations of (F.1), we get

$$\delta_{A_1} A_1 + \delta_{A_2} A_2 = \Lambda - \mu S^*$$

Once the above equation is satisfied, all the equations in system (F.1) hold. Therefore, there are infinitely many interior equilibria when  $\mathcal{R}_{0,1} = \mathcal{R}_{0,2} > 1$ .

#### References

Ahmed, I., Modu, G.U., Yusuf, A., Kumam, P., Yusuf, I., 2021. A mathematical model of Coronavirus disease (COVID-19) containing asymptomatic and symptomatic classes. Results Phys. 21, 103776.

Al-Darabsah, I., Yuan, Y., 2018. A periodic disease transmission model with asymptomatic carriage and latency periods. J. Math. Biol. 77 (2), 343–376.

Ali, M., Shah, S.T.H., Imran, M., Khan, A., 2020. The role of asymptomatic class, quarantine and isolation in the transmission of COVID-19. J. Biol. Dyn. 14 (1), 389-408

Anggriani, N., Ndii, M.Z., Amelia, R., Suryaningrat, W., Pratama, M.A.A., 2022. A mathematical COVID-19 model considering asymptomatic and symptomatic classes with waning immunity. Alex. Eng. J. 61 (1), 113–124.

Arruda, E.F., Das, S.S., Dias, C.M., Pastore, D.H., 2021. Modelling and optimal control of multi strain epidemics, with application to COVID-19. Plos One 16 (9), e0257512.

Bugalia, S., Bajiya, V.P., Tripathi, J.P., Li, M.-T., Sun, G.-Q., 2020. Mathematical modeling of COVID-19 transmission: The roles of intervention strategies and lockdown. Math. Biosci. Eng. 17 (5), 5961–5986.

Burki, T.K., 2022. Omicron variant and booster COVID-19 vaccines. Lancet Resp. Med. 10 (2), e17.

- Cai, L., Li, X., Tuncer, N., Martcheva, M., Lashari, A.A., 2017. Optimal control of a Malaria model with asymptomatic class and superinfection. Math. Biosci. 288, 94–108.
- Cai, L.-M., Martcheva, M., Li, X.-Z., 2013. Competitive exclusion in a vector-host epidemic model with distributed delay. J. Biol. Dyn. 7 (sup1), 47–67.
- Calleri, F., Nastasi, G., Romano, V., 2021. Continuous-time stochastic processes for the spread of COVID-19 disease simulated via a Monte Carlo approach and comparison with deterministic models. J. Math. Biol. 83 (4), 1–26.
- Centers for Disease Control and Prevention (CDC), 2022a. COVID data tracker. https://covid.cdc.gov/covid-data-tracker.
- Centers for Disease Control and Prevention (CDC), 2022b. Life expectancy for the US population. https://www.cdc.gov/nchs/fastats/life-expectancy.htm.
- Chisholm, R.H., Campbell, P.T., Wu, Y., Tong, S.Y., McVernon, J., Geard, N., 2018. Implications of asymptomatic carriers for infectious disease transmission and control. R. Soc. Open Sci. 5 (2), 172341.
- Dang, Y.-X., Li, X.-Z., Martcheva, M., 2016. Competitive exclusion in a multi-strain immuno-epidemiological influenza model with environmental transmission. J. Biol. Dyn. 10 (1), 416–456.
- de León, U.A.-P., Avila-Vales, E., Huang, K.-l., 2022. Modeling COVID-19 dynamic using a two-strain model with vaccination. Chaos Solitons Fractals 157, 111927.
- Duan, X.-C., Yin, J.-F., Li, X.-Z., Martcheva, M., 2018. Competitive exclusion in a multistrain virus model with spatial diffusion and age of infection. J. Math. Anal. Appl. 459 (2), 717–742.
- Fudolig, M., Howard, R., 2020. The local stability of a modified multi-strain SIR model for emerging viral strains. Plos One 15 (12), e0243408.
- Gao, S., Martcheva, M., Miao, H., Rong, L., 2021. A dynamic model to assess human papillomavirus vaccination strategies in a heterosexual population combined with men who have sex with men. Bull. Math. Biol. 83 (1), 1–36.
- Hart, W.S., Maini, P.K., Thompson, R.N., 2021. High infectiousness immediately before COVID-19 symptom onset highlights the importance of continued contact tracing. ELife 10, e65534.
- He, X., Lau, E.H., Wu, P., Deng, X., Wang, J., Hao, X., Lau, Y.C., Wong, J.Y., Guan, Y., Tan, X., et al., 2020. Temporal dynamics in viral shedding and transmissibility of COVID-19. Nat. Med. 26 (5), 672–675.
- He, S., Yang, J., He, M., Yan, D., Tang, S., Rong, L., 2021. The risk of future waves of COVID-19: Modeling and data analysis. Math. Biosci. Eng. 18 (5), 5409–5426.
- Head, J.R., Andrejko, K.L., Remais, J.V., 2022. Model-based assessment of SARS-CoV-2 Delta variant transmission dynamics within partially vaccinated K-12 school populations. Lancet Reg. Health-Am. 5, 100133.
- Howard, J., Huang, A., Li, Z., Tufekci, Z., Zdimal, V., van der Westhuizen, H.-M., von Delft, A., Price, A., Fridman, L., Tang, L.-H., et al., 2021. An evidence review of face masks against COVID-19. Proc. Natl. Acad. Sci. 118 (4), e2014564118.
- Hsu, S.-B., Hsieh, Y.-H., 2008. On the role of asymptomatic infection in transmission dynamics of infectious diseases. Bull. Math. Biol. 70 (1), 134–155.
- Huo, X., Chen, J., Ruan, S., 2021. Estimating asymptomatic, undetected and total cases for the COVID-19 outbreak in Wuhan: A mathematical modeling study. BMC Infect. Dis. 21 (1), 1–18.
- Iannelli, M., Martcheva, M., Li, X.-Z., 2005. Strain replacement in an epidemic model with super-infection and perfect vaccination. Math. Biosci. 195 (1), 23–46.
- Khan, M.A., Atangana, A., 2022. Mathematical modeling and analysis of COVID-19: A study of new variant Omicron. Physica A 127452.
- Knock, E.S., Whittles, L.K., Lees, J.A., Perez-Guzman, P.N., Verity, R., FitzJohn, R.G., Gaythorpe, K.A., Imai, N., Hinsley, W., Okell, L.C., et al., 2021. Key epidemiological drivers and impact of interventions in the 2020 SARS-CoV-2 epidemic in England. Sci. Transl. Med. 13 (602), 4262.
- Li, X.-Z., Gao, S.-S., Bhattacharya, S., 2013. A two-strain epidemic model with differential susceptibility and mutation. J. Biol. Systems 21 (04), 1340009.
- Li, X.-Z., Gao, S., Fu, Y.-K., Martcheva, M., 2021a. Modeling and research on an immuno-epidemiological coupled system with coinfection. Bull. Math. Biol. 83 (11), 1–42.
- Li, R., Li, Y., Liu, Y., Li, X., Zhuang, G., Shen, M., Zhang, L., et al., 2021b. Evaluating the impact of SARS-CoV-2 variants on the COVID-19 epidemic and social restoration in the United States: A mathematical modelling study. Front. Public Health 2067.
- Li, X.-Z., Liu, J.-X., Martcheva, M., 2010. An age-structured two-strain epidemic model with super-infection. Math. Biosci. Eng. 7 (1), 123.
- Liu, Y., Rocklöv, J., 2022. The effective reproduction number for the omicron SARS-CoV-2 variant of concern is several times higher than Delta. J. Travel Med. 29 (3), 037.
- Lovell-Read, F., Funk, S., Obolski, U., Donnelly, C., Thompson, R., 2021. Interventions targeting non-symptomatic cases can be important to prevent local outbreaks: SARS-CoV-2 as a case study. J. R. Soc. Interface 18, 20201014.
- Martcheva, M., 2007. On the mechanism of strain replacement in epidemic models with vaccination. In: Current Developments in Mathematical Biology. World Scientific, pp. 149–172.
- Martcheva, M., 2009. A non-autonomous multi-strain SIS epidemic model. J. Biol. Dyn. 3 (2–3), 235–251.
- Martcheva, M., 2015. An Introduction to Mathematical Epidemiology,Vol. 61. Springer. Martcheva, M., Bolker, B.M., Holt, R.D., 2008. Vaccine-induced pathogen strain replacement: What are the mechanisms? J. R. Soc. Interface 5 (18), 3–13.

- Martcheva, M., Iannelli, M., Li, X.-Z., 2007. Subthreshold coexistence of strains: The impact of vaccination and mutation. Math. Biosci. Eng. 4 (2), 287.
- Martcheva, M., Li, X.-Z., 2013. Competitive exclusion in an infection-age structured model with environmental transmission. J. Math. Anal. Appl. 408 (1), 225–246.
- Martcheva, M., Pilyugin, S.S., 2006. The role of coinfection in multidisease dynamics. SIAM J. Appl. Math. 66 (3), 843–872.
- Massard, M., Eftimie, R., Perasso, A., Saussereau, B., 2022. A multi-strain epidemic model for COVID-19 with infected and asymptomatic cases: Application to French data. J. Theoret. Biol. 111117.
- Mathieu, E., Ritchie, H., Ortiz-Ospina, E., Roser, M., Hasell, J., Appel, C., Giattino, C., Rodés-Guirao, L., 2021. A global database of COVID-19 vaccinations. Nat. Hum. Behav. 5 (7), 947–953.
- Murall, C.L., McCann, K.S., Bauch, C.T., 2014. Revising ecological assumptions about human papillomavirus interactions and type replacement. J. Theoret. Biol. 350, 98–109.
- Musa, S.S., Wang, X., Zhao, S., Li, S., Hussaini, N., Wang, W., He, D., 2022. The heterogeneous severity of COVID-19 in African countries: A modeling approach. Bull. Math. Biol. 84 (3), 1–16.
- Ngonghala, C.N., Iboi, E., Eikenberry, S., Scotch, M., MacIntyre, C.R., Bonds, M.H., Gumel, A.B., 2020. Mathematical assessment of the impact of non-pharmaceutical interventions on curtailing the 2019 novel Coronavirus. Math. Biosci. 325, 108364.
- Park, S.W., Cornforth, D.M., Dushoff, J., Weitz, J.S., 2020. The time scale of asymptomatic transmission affects estimates of epidemic potential in the COVID-19 outbreak. Epidemics 31, 100392.
- Poolman, E.M., Elbasha, E.H., Galvani, A.P., 2008. Vaccination and the evolutionary ecology of human papillomavirus. Vaccine 26, C25–C30.
- Qiu, Z., Kong, Q., Li, X., Martcheva, M., 2013. The vector-host epidemic model with multiple strains in a patchy environment. J. Math. Anal. Appl. 405 (1), 12–36.
- Robinson, M., Stilianakis, N.I., 2013. A model for the emergence of drug resistance in the presence of asymptomatic infections. Math. Biosci. 243 (2), 163–177.
- Rocha Filho, T., Moret, M., Chow, C., Phillips, J., Cordeiro, A., Scorza, F., Almeida, A.-C., Mendes, J., 2021. A data-driven model for COVID-19 pandemic–evolution of the attack rate and prognosis for Brazil. Chaos Solitons Fractals 152, 111359.
- Rong, L., Feng, Z., Perelson, A.S., 2007. Emergence of HIV-1 drug resistance during antiretroviral treatment. Bull. Math. Biol. 69 (6), 2027–2060.
- Rong, L., Ribeiro, R.M., Perelson, A.S., 2012. Modeling quasispecies and drug resistance in hepatitis C patients treated with a protease inhibitor. Bull. Math. Biol. 74 (8), 1789–1817.
- Saad-Roy, C.M., Wingreen, N.S., Levin, S.A., Grenfell, B.T., 2020. Dynamics in a simple evolutionary-epidemiological model for the evolution of an initial asymptomatic infection stage. Proc. Natl. Acad. Sci. 117 (21), 11541–11550.
- Saucedo, O., Martcheva, M., 2017. Competition between low and high pathogenicity avian influenza in a two-patch system. Math. Biosci. 288, 52-70.
- Serhani, M., Labbardi, H., 2021. Mathematical modeling of COVID-19 spreading with asymptomatic infected and interacting peoples. J. Appl. Math. Comput. 66 (1), 1–20.
- Shen, M., Zu, J., Fairley, C.K., Pagán, J.A., An, L., Du, Z., Guo, Y., Rong, L., Xiao, Y., Zhuang, G., et al., 2021a. Projected COVID-19 epidemic in the United States in the context of the effectiveness of a potential vaccine and implications for social distancing and face mask use. Vaccine 39 (16), 2295–2302.
- Shen, M., Zu, J., Fairley, C.K., Pagán, J.A., Ferket, B., Liu, B., Yi, S.S., Chambers, E., Li, G., Guo, Y., et al., 2021b. Effects of New York's executive order on face mask use on COVID-19 infections and mortality: A modeling study. J. Urban Health 98 (2), 197–204.
- Sonabend, R., Whittles, L.K., Imai, N., Perez-Guzman, P.N., Knock, E.S., Rawson, T., Gaythorpe, K.A., Djaafara, B.A., Hinsley, W., FitzJohn, R.G., et al., 2021. Non-pharmaceutical interventions, vaccination, and the SARS-CoV-2 delta variant in England: A mathematical modelling study. Lancet 398 (10313), 1825–1835.
- Srivastav, A.K., Tiwari, P.K., Srivastava, P.K., Ghosh, M., Kang, Y., 2021. A mathematical model for the impacts of face mask, hospitalization and quarantine on the dynamics of COVID-19 in India: deterministic vs. stochastic. Math. Biosci. Eng. 18 (1), 182–213.
- Subramanian, R., He, Q., Pascual, M., 2021. Quantifying asymptomatic infection and transmission of COVID-19 in New York city using observed cases, serology, and testing capacity. Proc. Natl. Acad. Sci. 118 (9), e2019716118.
- Tang, K.H.D., 2022. Movement control as an effective measure against Covid-19 spread in Malaysia: An overview. J. Public Health 30 (3), 583–586.
- Thomasey, D.H., Martcheva, M., 2008. Serotype replacement of vertically transmitted diseases through perfect vaccination. J. Biol. Systems 16 (02), 255–277.
- Van den Driessche, P., Watmough, J., 2002. Reproduction numbers and sub-threshold endemic equilibria for compartmental models of disease transmission. Math. Biosci. 180 (1–2), 29–48.
- World Health Organization, 2022. COVID facts. https://www.who.int/health-topics/coronavirus.
- Zhang, M., Xiao, J., Deng, A., Zhang, Y., Zhuang, Y., Hu, T., Li, J., Tu, H., Li, B., Zhou, Y., et al., 2021. Transmission dynamics of an outbreak of the COVID-19 Delta variant B 1.617. 2-Guangdong province, China, may–2021. Chin. CDC Weekly 3 (27), 584.